

Discovery of a Highly Unequal-Mass Binary T Dwarf with Keck Laser Guide Star Adaptive Optics: A Coevality Test of Substellar Theoretical Models and Effective Temperatures¹

Michael C. Liu,² Trent J. Dupuy,² and S. K. Leggett³

ABSTRACT

Highly unequal-mass ratio binaries are rare among field brown dwarfs, with the mass ratio distribution of the known census described by $q^{(4.9\pm 0.7)}$. However, such systems enable a unique test of the joint accuracy of evolutionary and atmospheric models, under the constraint of coevality for the individual components (the “isochrone test”). We carry out this test using two of the most extreme field substellar binaries currently known, the T1+T6 ϵ Ind Bab binary and a newly discovered 0.14'' T2.0+T7.5 binary, 2MASS J12095613–1004008AB, identified with Keck laser guide star adaptive optics. The latter is the most extreme tight binary resolved to date ($q \approx 0.5$). Based on the locations of the binary components on the H-R diagram, current models successfully indicate that these two systems are coeval, with internal age differences of $\log(\text{age}) = -0.8 \pm 1.3$ ($-1.0^{+1.2}_{-1.3}$) dex and $0.5^{+0.4}_{-0.3}$ ($0.3^{+0.3}_{-0.4}$) dex for 2MASS J1209–1004AB and ϵ Ind Bab, respectively, as inferred from the Lyon (Tucson) models. However, the total mass of ϵ Ind Bab derived from the H-R diagram ($\approx 80 M_{\text{Jup}}$ using the Lyon models) is strongly discrepant with the reported dynamical mass. This problem, which is independent of the assumed age of the ϵ Ind Bab system, can be explained by a ≈ 50 – 100 K systematic error in the model atmosphere fitting, indicating slightly warmer temperatures for both components; bringing the mass determinations from the H-R diagram and the visual orbit into consistency leads to an inferred age of ≈ 6 Gyr for ϵ Ind Bab, older than previously assumed. Overall, the two T dwarf binaries studied here, along with recent results from T dwarfs in age and mass benchmark systems, yield evidence for small (≈ 100 K) errors in the evolutionary models and/or model atmospheres, but not significantly larger. Future parallax, resolved

¹Most of the data presented herein were obtained at the W.M. Keck Observatory, which is operated as a scientific partnership among the California Institute of Technology, the University of California, and the National Aeronautics and Space Administration. The Observatory was made possible by the generous financial support of the W.M. Keck Foundation.

²Institute for Astronomy, University of Hawai‘i, 2680 Woodlawn Drive, Honolulu, HI 96822; mliu@ifa.hawaii.edu

³Gemini Observatory, 670 North A‘ohoku Place, Hilo, HI 96720

spectroscopy, and dynamical mass measurements for 2MASS J1209–1004AB will enable a more stringent application of the isochrone test. Finally, the binary nature of this object reduces its utility as the primary T3 near-IR spectral typing standard; we suggest SDSS J1206+2813 as a replacement.

Subject headings: binaries: general, close — stars: brown dwarfs — infrared: stars — techniques: high angular resolution

1. Introduction

Wide-field surveys have now identified nearly a thousand ultracool dwarfs (spectral types later than M6) in the solar neighborhood, spanning temperatures and (inferred) masses that range from the stellar/substellar boundary defined by the hydrogen-burning minimum mass ($\approx 75 M_{\text{Jup}}$), down to the proposed substellar/planetary boundary demarcated by the deuterium-burning limit ($\approx 13 M_{\text{Jup}}$). This census has enabled extensive characterization of the spectrophotometric properties of these low-luminosity, low-temperature objects. However, studies of the substellar field population are inevitably hindered by the unknown properties of individual objects, making it difficult to disentangle the effects of varying ages, masses, and compositions on the underlying physics. In principle, a sample of star clusters with complete membership down to very low masses and encompassing a range of ages would be ideal. However, such a sensitive census only exists for a handful of young (\sim few Myr) clusters (e.g. Lodieu et al. 2007; Luhman et al. 2007a), where the lowest mass members are easiest to detect. With increasing age, dynamical evolution leads to depletion of the lowest mass members such that older clusters may be largely devoid of brown dwarfs (Adams et al. 2002; Bouvier et al. 2008).

One avenue for circumventing these limitations is through the study of binary brown dwarfs, as binaries constitute systems of common (albeit unknown) age and metallicity. About 15% of field brown dwarfs are tight binary systems, resolved largely by *Hubble Space Telescope* or ground-based adaptive optics (AO) imaging and composed mostly of nearly equal-luminosity (and thus equal-mass) components (e.g. Burgasser et al. 2007). These “mini-clusters” have proven to be fertile ground for understanding the physical processes that govern the emergent spectra of brown dwarfs (e.g. Liu & Leggett 2005; Liu et al. 2006; Burgasser et al. 2006d) and for testing theoretical models with dynamical mass determinations (e.g. Zapatero Osorio et al. 2004; Ireland et al. 2008; Liu et al. 2008; Dupuy et al. 2009c; Konopacky et al. 2010; Dupuy et al. 2010).

As part of our ongoing program to study the multiplicity and physical properties of substellar binaries using laser guide star adaptive optics (LGS AO), we present here the discovery of the binarity of 2MASS J12095613–1004008, hereinafter 2MASS J1209–1004. This object was identified in 2MASS data by Burgasser et al. (2004) and spectrally typed by them and by Chiu et al. (2006) as a T3 dwarf based on integrated-light near-IR spectroscopy. Burgasser et al. (2006b) define 2MASS J1209–1004 as the primary T3 spectral type standard for their near-IR classification

scheme for T dwarfs. This object has not previously been targeted with high angular resolution imaging. What distinguishes 2MASS J1209–1004AB from most previously known substellar field binaries is the large IR brightness difference between its two components, indicating an atypical mass ratio compared to the plethora of nearly equal-mass binaries. As we describe below, 2MASS J1209–1004AB provides a new opportunity to test theoretical models of brown dwarfs — by requiring the model-derived ages of the two components to be consistent with coevality of the system, an approach which we refer to here as the “isochrone test.”

2. Observations

We imaged 2MASS J1209–1004 on 22 April 2007 and 16 January 2008 UT using the sodium LGS AO system of the 10-meter Keck II Telescope on Mauna Kea, Hawaii (Wizinowich et al. 2006; van Dam et al. 2006). We used the facility IR camera NIRC2 with its narrow field-of-view camera, which produces a $10.2'' \times 10.2''$ field of view. Conditions were photometric for both runs. The LGS provided the wavefront reference source for AO correction, with the tip-tilt motion measured contemporaneously from the $R = 14.7$ mag field star USNO-B1.0 0799-0230529 (Monet et al. 2003) located $68''$ away from 2MASS J1209–1004. The LGS brightness, as measured by the flux incident on the AO wavefront sensor, was equivalent to a $V \approx 9.6 - 10.0$ mag star. In April 2007, we obtained images with the MKO J ($1.25 \mu\text{m}$), H ($1.64 \mu\text{m}$), and K ($2.20 \mu\text{m}$) filters. In January 2008, we obtained images with the CH_4s filter, which has a central wavelength of $1.592 \mu\text{m}$ and a width of $0.126 \mu\text{m}$.

The images were analyzed in the same fashion as our previous LGS papers (Liu et al. 2008, 2006). The raw images were reduced using standard methods of flat-fielding and sky-subtraction. The binary’s flux ratios and relative astrometry were derived by fitting an analytic model of the point spread function (PSF) as the sum of three elliptical gaussians. The measurements were made on the individual images, with outlier images of much poorer quality excluded. The averages of the fitting results were adopted as the final measurements and the standard deviations as the errors. The final flux ratios were used to correct the Strehl ratio measurements of the images for the contamination from the light of the secondary component. We did not correct the relative astrometry for instrumental optical distortion, as the size of the effect as predicted from a distortion solution by B. Cameron (priv. comm.) is insignificant compared to our measurements uncertainties.

In order to validate our measurements, we created myriad artificial binary stars from LGS images of single stars with comparable Strehl and FWHM as the science data. For each filter, our fitting code was applied to artificial binaries with similar separations and flux ratios as 2MASS J1209–1004AB over a range of PAs. The simulations showed that the random errors are reasonable and any systematic offsets are small. In cases where the measurement errors from the artificial binaries were larger than those from the 2MASS J1209–1004AB measurements, we conservatively adopted the larger errors.

We adopted a pixel scale of 9.963 ± 0.005 mas/pixel and an orientation for the detector’s $+y$ axis of $+0.13 \pm 0.07^\circ$ for NIRC2 as determined by Ghez et al. (2008). We computed the expected shift in the relative astrometry of the two components due to differential chromatic refraction (DCR) in the same manner as in our previous work (e.g. Dupuy et al. 2009c). The DCR effects are small ($\approx 1\text{--}3$ mas) compared to the measurement errors, and therefore we did not account for them. Table 1 presents our final Keck LGS measurements, and Figure 1 shows our Keck LGS images.

3. Results for 2MASS J1209–1004AB

3.1. Proof of Companionship

The near-IR broadband colors of 2MASS J1209–1004B are extremely blue, which provides strong circumstantial evidence that it is a physically associated late-T dwarf companion and not a background object. Burgasser et al. (2004) measure a proper motion for 2MASS J1209–1004 of $0.46 \pm 0.10''/\text{yr}$ at a PA of $140 \pm 8^\circ$. Considering this proper motion, examination of the Digitized Sky Survey images shows no plausible optical counterpart if component B were a background object. Our two epochs of Keck LGS imaging separated by 9 months are consistent with no change in the relative position of the two components. If the companion were a background object, in Jan 2008 the system should have had a separation of $0.48 \pm 0.07''$ at a PA of $317 \pm 6^\circ$, which is 4.8σ discrepant with the observed separation, neglecting the effect of parallax. Finally, our LGS photometry indicates the presence of H -band methane absorption in component B (§ 3.2), inconsistent with the background star hypothesis. Thus both the astrometry and photometry independently indicate that the system is a true physical binary.

3.2. Resolved Photometry

We use our measured flux ratios and the published JHK photometry from Chiu et al. (2006) to derive resolved IR colors and magnitudes for 2MASS J1209–1004AB on the MKO system. For the CH_4s data, we synthesize integrated-light photometry of 15.05 ± 0.03 mag from the near-IR spectrum of Burgasser et al. (2004), flux-calibrated to the broadband MKO photometry of $H = 15.24 \pm 0.03$ mag. We assume that the components of 2MASS J1209–1004AB are themselves single, not unresolved binaries. Table 2 presents the resolved photometry. Comparing to known ultracool dwarfs, Figure 2 shows that component A has IR colors most typical of T2–T3 dwarfs. The uncertainties are larger for component B, but its near-IR colors appear to be comparable or even bluer than the very latest T dwarfs.

The resolved ($CH_4s - H$) colors provide more accurate estimates of the spectral types than the broadband colors, as the H -band methane absorption correlates well with overall near-IR spectral type (e.g., Figure 2 of Tinney et al. 2005). We convert these colors to near-IR spectral type using

the polynomial fit from Liu et al. (2008):

$$SpT = 19.40 - 19.698 \times (CH_4s - H) - 8.3600 \times (CH_4s - H)^2 \quad (1)$$

where $SpT = 20$ for T0, $= 21$ for T1, etc. The RMS scatter about the fits is 0.3 subclasses. The fit was originally derived for objects from T0 to T8, but as discussed below the more recently discovered T9 objects are still well-described by this relation.

The observed $(CH_4s - H)$ colors for 2MASS J1209–1004AB give spectral types of $T1.6 \pm 0.9$ and $T9 \pm 2$ for components A and B, respectively, where the spectral type uncertainties come from propagation of the errors in the colors. Note that the $(CH_4s - H)$ color of component B (-0.8 ± 0.3 mag) is bluer than any of the objects used to define the polynomial fit, so the spectral type estimate represents a small extrapolation of the relation. For comparison, the colors of the T8.5 dwarfs ULAS 1238+0953 and ULAS 2146–0010 are -0.65 and -0.63 mags, respectively, and those of the T9 dwarfs ULAS 0034–0052, CFBDS 0059–0114, and ULAS 1335+1130 are -0.56 , -0.63 , and -0.66 mags, respectively, as synthesized from their published near-IR spectra (Warren et al. 2007; Delorme et al. 2008; Burningham et al. 2008, 2009). (These very late-T dwarfs are not included in the Liu et al. fit, but their inclusion would make no significant difference in the polynomial relation.) Overall, component B shows H -band methane absorption comparable to the latest known T dwarfs.

3.3. Composite Spectra and Resolved Spectral Types

We modeled the integrated-light spectrum of 2MASS J1209–1004 as the composite sum of two template T dwarfs, as an additional means to determine the resolved spectral types. The templates were chosen from available near-IR spectra for dwarfs that have similar colors to those of 2MASS J1209–1004 A and B. We produced various fits using SDSS J0758+3247 (T2; Knapp et al. 2004), SDSS J1254–0122 (T2; Leggett et al. 2000) and SDSS J1521+0131 (T2; Knapp et al. 2004) as templates for the component A and Gl 570D (T7.5; (Burgasser et al. 2000)), 2MASS J0415–0935 (T8; Burgasser et al. 2002), ULAS J1017+0118 (T8p; Burningham et al. 2008) and ULAS J1315+0826 (T7.5; Pinfield et al. 2008) as templates for component B. The JHK colors of the template dwarfs and the resolved binary are within 0.2 mag for the component A and 0.4 mag for the component B (whose observed photometry is much more uncertain).

Before combining each template pair, we scaled each template spectrum to a distance of 10 pc. Trigonometric parallaxes are known for SDSS J1254–0122 and 2MASS J0415–0935. For the other dwarfs distances were estimated using the relationships between absolute magnitudes and spectral type from Liu et al. (2006). We explored fits using both the "bright" and "faint" relations, which differ significantly for early-type T dwarfs. For each pair, after shifting the flux to 10pc, the flux at each wavelength was summed, and the result compared to the observed unresolved spectrum for 2MASS J1209–1004AB. There is no parallax measurement for 2MASS J1209–1004AB, and

so we shifted the observed spectrum to that of the synthesized spectrum, determined the implied distance, and compared the resulting spectra.

In the end, model composite spectra composed of a T2 primary and T7.5 secondary showed good agreement with the observed integrated-light spectrum (Figure 3). Any combination using the peculiar T8 dwarf ULAS J1017+0118 failed to reproduce the observed strength of the CH_4 feature at $1.6 \mu\text{m}$. The best fits were obtained using the T2 dwarf SDSS J1254–0122 in combination with either of the T7.5 dwarfs Gl 570D or ULAS J1315+0826, or using the T2 dwarf SDSS J1521+0131 in combination with the T8 dwarf 2MASS J0415–0935. For the last combination to work, the distance for SDSS J1521+0131 must be derived using the "faint" Liu et al. photometric relation. The implied distance for 2MASS J1209–1004AB is 23 pc from the SDSS J1254–0122 fits, or 18 pc from the SDSS J1521+0131 fit.

Combining the results from the JHK and $(\text{CH}_4s - H)$ colors and this spectral modeling, we adopt a spectral type of $\text{T}2 \pm 0.5$ for 2MASS J1209–1004A, as all the available estimates are in good agreement.

The typing for component B is more challenging, given its larger photometric errors and its relative faintness (and thus modest contribution to the integrated-light spectrum). In the spectral modeling, T7.5 templates provided the best matches. Our attempts to use T8 dwarfs failed to produce a good match, though this was possibly limited by the small number of templates with comparably blue near-IR colors as 2MASS J1209–1004B (2MASS J0415–0935 and ULAS J1017+0118). The polynomial fits for absolute magnitude as a function of spectral type from Liu et al. (2006) give $M(J) = \{15.1, 15.5, 15.9, 16.3\}$ mag, $M(H) = \{15.5, 15.9, 16.3, 16.7\}$ mag, and $M(K) = \{15.6, 16.0, 16.4, 16.7\}$ mag for near-IR spectral types of T6.5, T7, T7.5, and T8, respectively. Based on the photometric distance to component A (§ 3.5), the absolute magnitudes of component B are $M(J, H, K) = 15.7 \pm 0.4, 16.5 \pm 0.5, 16.9 \pm 0.7$ mag, in good agreement with T7.5. Given the concordance between this and the spectral modeling, we adopt a spectral type estimate of $\text{T}7.5 \pm 0.5$ for component B.

3.4. T3 Near-IR Spectral Type Standard

Burgasser et al. (2006b) chose 2MASS J1209–1004 as the primary T3 spectral standard for near-IR classification of T dwarfs. Its binary nature now lessens its utility for this purpose, especially at the bluer wavelengths where the contribution of the secondary to the integrated-light spectrum is greater. The secondary standard proposed by Burgasser et al. was SDSS J1021–0304AB, which also has been resolved into a binary (T1+T5; Burgasser et al. 2006d). For both sources, their binary nature make them unappealing as the T3 spectral standard, since the secondary contributes significantly to the integrated near-infrared light (e.g., Figure 3).¹ Furthermore the

¹The mid-infrared regime becomes increasingly dominant for cooler T dwarfs (e.g. Figure 3 of Cushing et al.

primary of neither system is of T3 type. Options for a different spectral standard are limited, due to the modest number of T3 dwarfs known. At the relatively brighter magnitudes, the choices are SDSS J120602.51+281328.7 (T3; $J = 16.5$ mag) and SDSS J141530.05+572428.7 (T3±1; $J = 16.7$), both of which were identified and classified by Chiu et al. (2006). SDSS J1206+2813 appears to be single in $0.06''$ FWHM images obtained by us with Keck LGS (Liu et al., in prep.) while no high angular resolution imaging is available yet for SDSS J1415+5724. As the individual spectral indices for SDSS J1206+2813 are more consistent with a T3 typing and it appears to be single, we suggest that it be used as the T3 spectral standard.

3.5. Photometric Distance

With an estimated spectral type of $T2.0 \pm 0.5$ for component A, we use the Liu et al. (2006) polynomial fits of absolute magnitude as a function of spectral type to determine a photometric distance. We use the J -band photometry; the H and K -band data produce nearly identical results but with somewhat larger uncertainties. Errors in the photometric distance include the uncertainties in the apparent magnitude (0.05 mag), the uncertainty in J -band absolute magnitude arising from the spectral type uncertainty (0.05 mag), and the intrinsic dispersion about the fit (0.4 mag). Liu et al. provide both a “bright” and a “faint” relation, depending on the inclusion or exclusion of candidate overluminous objects of early/mid-T spectral type, respectively. The two relations give consistent answers within the errors, 24 ± 4 and 18 ± 4 pc, respectively. We average to arrive at a final photometric distance of 21 ± 4 pc.²

Since the spectral templates used for modeling the composite spectra have distance determinations (§ 3.3), the scaling factor used to match to 2MASS J1209–1004AB also provides a distance estimate to the binary, with a value of 18 or 23 pc (§ 3.3). An error estimate from this approach is uncertain. The T2 dwarf SDSS J1254–0122 (Leggett et al. 2000) provides a well-matching template for component A and has parallax with an uncertainty of 4% (Vrba et al. 2004), which represents the very smallest possible uncertainty. At the other extreme, the photometric relations of Liu et al. (2006) have a RMS scatter about the fit of 15–20% in distance. Adopting a distance error of 10% is a reasonable compromise; for instance, Liu et al. demonstrate that fitting the composite spectrum of the T1+T6 binary ϵ Ind Bab produces a distance estimate that agrees to 10% with the measured parallax. Thus, the distance estimates from the spectral modeling agree with the photometric distance of 21 ± 4 pc. We conservatively adopt the latter in our subsequent analysis.³

2006) and so the T7.5 2MASS J1209–1004B is also expected to make a significant contribution to the integrated 2MASS J1209–1004 flux at $\sim 10 \mu\text{m}$.

²In a similar fashion, we find a photometric distance to component B of 19 ± 5 pc based on its type of $T7.5 \pm 0.5$. This value is consistent with the distance derived component A, but it cannot be considered truly an independent measurement, since we use the photometric distance in estimating the spectral type for component B in § 3.3.

³The slightly larger distance from the spectral modeling results from the fact that SDSS J1254–0122 is slightly

3.6. Bolometric Luminosities

3.6.1. Combined System

There is no published value for the integrated-light bolometric luminosity of 2MASS J1209–1004, so we computed it directly from its near-IR spectrum (Burgasser et al. 2004), flux calibrated with the Chiu et al. (2006) photometry, and combined with mid-IR photometry. For the latter, IRAC photometry is available in the *Spitzer* archive, obtained as part of the Cycle 1 GTO program 35 on UT 2005 June 13. Exposure times were 30 s, and a 5-position small dither pattern was used. The binary is unresolved in the IRAC images, and an 8" aperture was used for the photometry. We determined magnitudes of $[3.6] = 14.02 \pm 0.004$, $[4.5] = 13.49 \pm 0.004$, $[5.8] = 13.33 \pm 0.016$, and $[8.0] = 13.06 \pm 0.06$ mags. A 0.03 mag error should be added in quadrature to the quoted random errors to account for systematic effects.

To derive the integrated-light L_{bol} , we numerically integrated the near-IR spectrum and the mid-IR photometry, interpolating between the gaps in the data, extrapolating at shorter wavelengths to zero flux at zero wavelength, and extrapolating beyond $4.5 \mu\text{m}$ assuming a blackbody. We determined the luminosity error in a Monte Carlo fashion, by adding randomly drawn noise to our data over many trials and computing the rms of the resulting luminosities. In this process, we accounted for the noise in the spectrum, the errors in the MKO photometry used to flux-calibrate it, and the errors in our mid-IR photometry estimates. Before accounting for the error in the photometric distance, we found a total bolometric luminosity of $\log(L_{\text{bol}}/L_{\odot}) = -4.61 \pm 0.02$ dex. With the 20% uncertainty in the photometric distance included, the L_{bol} uncertainty becomes 0.15 dex.

3.6.2. Individual Components

To compute the bolometric luminosities (L_{bol}) for each component, we apply bolometric corrections to the resolved near-IR photometry based on the compilation in Appendix A. Despite the relatively larger RMS about the *BC* fit at *J*-band, the photometry of the component B is most accurately determined in this bandpass, so we use it to determine L_{bol} and associated quantities. The results are given in Table 2. The L_{bol} uncertainties are composed of the uncertainties from the apparent magnitudes, from the bolometric corrections arising from the spectral type uncertainty, the intrinsic dispersion about our polynomial fits, and the photometric distance. The last item dominates the uncertainties in the L_{bol} values. (However, the luminosity *ratio* of two components is known to much higher precision than the individual L_{bol} values, since the ratio is independent

brighter than the values from the adopted Liu et al. polynomial fits. In fact, it has been suggested this system may be a binary based on this modest overluminosity (Liu et al. 2006; Burgasser 2007), though it has not been resolved as such in high angular resolution imaging from *HST* or Keck LGS AO (Burgasser et al. 2006d; Liu et al. in prep.) and modeling of its integrated-light spectra suggests the system is more likely be a relatively young, single object as opposed to a near-equal mass binary (Stephens et al. 2009).

of the distance uncertainty.) As a consistency check, we note that the sum of the individual component luminosities derived from BC_J (-4.51 ± 0.18 dex) agrees well with the direct computation from the integrated light spectrum (-4.61 ± 0.15 dex).

3.7. Physical Properties from Evolutionary Models

With the L_{bol} determinations for the individual components and an assumed age, evolutionary models can then fully determine the physical properties of the two components (e.g. Saumon et al. 2000). Figure 4 shows the results graphically using the Burrows et al. (1997) evolutionary models, where we have adopted a generic age range of 0.1–10 Gyr for the 2MASS J1209–1004AB system. The figure indicates the complete possible set of $\{T_{\text{eff}}, \log(g)\}$ values for the two components, based on our L_{bol} determinations.

Table 3 summarizes the physical properties derived from this approach, for a range of assumed ages. Note that for computing relative quantities between the components (e.g., luminosity ratio and mass ratio), we take care to account for the covariance of the measurements due to the fact that the uncertainty in the distance is common to both components, and thus uncertainties in these relative quantities are smaller than for the absolute value of these quantities for the individual components. To do this, we draw values for all the relevant measurements in a Monte Carlo fashion, keeping track of all the calculations of the physical parameters in every trial, and then compute the final result and RMS from the ensemble of trials.

To compute the estimated orbital period of the system, following Torres (1999), we assume random viewing angles and a uniform eccentricity distribution from $e = 0 - 1$. This gives a multiplicative correction factor of $1.10_{-0.36}^{+0.91}$ (68.3% confidence limits) for converting the projected separation into a semi-major axis. The estimated orbital periods range from 16–26 years for ages of 0.5, 1.0, and 5.0 Gyr, albeit with significant uncertainties. Dynamical masses for ultracool binaries are possible from orbital monitoring covering $\gtrsim 30\%$ of the orbital period (e.g. Bouy et al. 2004; Liu et al. 2008). Thus, 2MASS J1209–1004AB warrants continued high angular resolution imaging to determine its visual orbit, combined with a parallax measurement to compute its total mass.

4. Discussion: The Isochrone Test

The 2MASS J1209–1004AB system is a rare example of an ultracool binary with a highly unequal mass ratio ($q \approx 0.5$), as most ultracool binaries are composed of nearly equal components (Table 4). This novelty is highlighted in Figure 5, which shows the estimated mass ratios of all known field brown dwarf binaries, where we choose field systems in which the primary has an estimated spectral type of L4 or later as a proxy for the stellar/substellar boundary (Kirkpatrick et al. 1999). As explained below, we specifically focus on ultracool binaries composed of two brown dwarfs, as opposed to those that contain one or two very low-mass stars.

Under the conservative assumption of coequality, we can use 2MASS J1209–1004AB to test current theoretical models of brown dwarfs, by assessing whether the two components lie along a single isochrone on the Hertzsprung-Russell (H-R) diagram. We essentially treat the system as a star cluster composed of two members, with an unknown age but requiring that it is the same for components A and B. Hereinafter, we refer to this approach as the “isochrone test.”

Placement on the H-R diagram requires L_{bol} and T_{eff} . The former can be well-determined for ultracool dwarfs (Appendix A and references therein). However, robust temperature determinations are still an active area of investigation (e.g. Cushing et al. 2008). Atmospheric models for L and T dwarfs have not been confirmed by direct measurement of brown dwarf radii, only checked for consistency against evolutionary models using single brown dwarfs that are companions to stars of known age (e.g. Saumon et al. 2006; Leggett et al. 2008) and the few brown dwarf binaries with dynamical mass determinations (e.g. Liu et al. 2008; Dupuy et al. 2009b,c).⁴ Modelling low-temperature atmospheres is challenging. The molecular opacity line list for CH_4 , a species important for both the L and T dwarfs, is incomplete or non-existent below $1.6 \mu\text{m}$. The FeH line list is incomplete in the $1.2\text{--}1.3 \mu\text{m}$ region, which is important for L dwarfs. NH_3 is important for very late-type T dwarfs, but there are no opacities calculated below $1.4 \mu\text{m}$. Also, calculation of the very strongly pressure-broadened K I resonance doublet ($0.78 \mu\text{m}$) is difficult, and hence models do not currently reproduce the far-red region of T dwarf spectra very well. Finally, the treatment of the grains condensates is difficult, which impacts the $1.0\text{--}1.6 \mu\text{m}$ region of $\approx\text{L3}$ to $\approx\text{T2}$ types.

Thus, our current ability to carry out the isochrone test represents a test of the *joint* accuracy of evolutionary and atmospheric models, not of either specific class of models.⁵ The fact that the isochrone test relies on components of very different masses also may make it a useful signpost for mass-dependent problems, which would not be revealed when studying the (much more common) nearly-equal mass binaries. Of course, the coequality requirement is widely applied in studies of star clusters. Its particular characteristic in the case of substellar binaries arises from the fact that brown dwarfs steadily cool over their lifetime, and thus the isochrones for substellar objects are more dispersed on the H-R diagram compared to stellar isochrones.⁶

⁴Of course, for this purpose we cannot use temperatures that are derived from the evolutionary models themselves (e.g. Golimowski et al. 2004a), where the observed L_{bol} , an assumed age, and the evolutionary-model-derived radii are used to compute T_{eff} . If we did, then any information gleaned from the H-R diagram positions would automatically agree with the evolutionary models, i.e., this would partly be circular reasoning.

⁵One limitation on the isochrone test is that the currently available evolutionary models do not typically incorporate the same set of model atmospheres used in fitting observed spectra. However, Chabrier et al. (2000) show that the predicted luminosity evolution is mostly robust against the adopted model atmosphere.

⁶The isochrone test described here is conceptually identical to some previous studies of young star-forming regions. Although the underlying physical processes are different for pre-main sequence stars and field brown dwarfs, the luminosities of both classes of objects are strongly dependent on age. For young regions, coequality has been used to check the accuracy of evolutionary models and the spectral type-to-effective temperature scale, using multiple systems (e.g. Hartigan et al. 1994; White et al. 1999; Schaefer et al. 2008; Kraus & Hillenbrand 2009) and entire clusters (e.g. Luhman 1999). Note for such young objects, a complicating factor is the possible impact of accretion on the H-R

4.1. 2MASS J1209–1004AB

We now subject 2MASS J1209–1004AB to the isochrone test. A parallax measurement is not available, so we use the photometric distance estimate (§ 3.5) — this is not a limiting factor in the analysis. For the effective temperatures of each component, we consider previous analysis of the spectra for similarly typed T dwarfs.

Three T2 dwarfs have been analyzed in such a fashion: SDSS J0758+3247 (1100–1200 K; Stephens et al. 2009), SDSS J1254–0122 (1100–1200 K; Stephens et al. 2009; Cushing et al. 2008), and HN Peg B (1115 K; Leggett et al. 2008).⁷ The model atmospheres were spaced by 100 K (except for HN Peg B), and the estimated systematic uncertainties are ≈ 100 K due to, e.g., flux calibration, choice of wavelength region for fitting, and weighting scheme. Thus we adopt 1150 ± 100 K as the temperature for 2MASS J1209–1004A. No T1 or T3 dwarfs have been subjected to such analysis, but the T_{eff} fitted for early/mid-T dwarfs are all relatively constant (e.g. Stephens et al. 2009), in accord with the T_{eff} measurements derived from L_{bol} data that the L/T transition for field objects occurs at nearly constant temperature (e.g. Golimowski et al. 2004a).

Four T7.5 dwarfs have been analyzed to date: HD 3651B (820–830 K; Leggett et al. 2007), 2MASS J1114–2618 (725–775 K; Leggett et al. 2007), Gl 570 D (800–821 K; Saumon et al. 2006), and 2MASS J1217–0311 (850–950 K; Saumon et al. 2007). To encompass the potential uncertainty in the spectral type of component B, we also consider the T8 dwarf 2MASS J0415–0935 (725–775 K, 710 ± 40 K; Saumon et al. 2007; Burgasser et al. 2008b).⁸ No T7 dwarfs have independently determined T_{eff} ’s.⁹ Taking the unweighted mean and RMS of the results gives $T_{\text{eff}} = 800 \pm 70$ K as our adopted value for 2MASS J1209–1004B.

Figure 6 shows 2MASS J1209–1004AB on the H-R diagram. We compute the individual component ages based on their H-R diagram positions relative to the Lyon/COND (Baraffe et al. 2003) and Tucson (Burrows et al. 1997) evolutionary models, using a Monte Carlo method to account for the uncertainties. For each component, we draw trial values for L_{bol} and T_{eff} from a normal distribution, which are then used with finely interpolated tabulations of the models to derive a set of ages. We then take the difference of the component ages and compile the distribution

diagram positions (Baraffe et al. 2009), an effect which is not relevant for old (field) brown dwarfs.

⁷The first two objects were analyzed with direct fitting of model atmospheres to their observed spectra. For HN Peg B, the model atmosphere matching the T_{eff} derived from evolutionary models was shown to be consistent with the observed flux-calibrated spectrum.

⁸For Gl 570D and 2MASS J0415–0935, the model atmosphere matching the T_{eff} derived from evolutionary models was shown to be consistent with the observed flux-calibrated spectrum, as opposed to directly fitting model atmospheres to the spectra.

⁹Burgasser et al. (2006a) have determined T_{eff} ’s for a sample of mid/late-T dwarfs based on multi-band flux ratios measured from low-resolution near-IR spectra. However, these are calibrated against the T_{eff} and $\log(g)$ of Gl 570D derived directly from evolutionary models. And thus these T_{eff} ’s cannot be used to place objects on the H-R diagram, since this would be circular reasoning.

resulting from 10^6 trials.¹⁰ Figure 7 plots the result, which is well-described by a gaussian. Table 5 gives the derived ages and age difference. At the 1σ level, the models successfully indicate that the two components are coeval, with a $\log(\text{age})$ difference of $-0.8_{-1.3}^{+1.3}$ and $-1.0_{-1.3}^{+1.2}$ dex inferred from the Lyon and Tucson models, respectively.

4.2. ϵ Ind Bab

We also apply the isochrone test to the ϵ Ind Bab system, which is a wide (1459 AU) separation binary companion to the K5 V star ϵ IndA (Scholz et al. 2003). The binary is composed of a T1 and a T6 component (McCaughrean et al. 2004; Burgasser et al. 2006b), with a K -band flux ratio of 2.18 ± 0.03 mag. The system is quite similar to 2MASS J1209–1004AB, but with more precisely determined physical parameters and therefore offers a more stringent application of the isochrone test.¹¹

For the L_{bol} of the two components, we use the results from King et al. (2010) of $\log(L_{\text{bol}}/L_{\odot}) = -4.699 \pm 0.017$ and -5.232 ± 0.020 . Their measurements come from integrating the resolved spectra of the two components from optical to mid-IR wavelengths.¹²

The effective temperatures of the two components have been derived by fitting model atmospheres by two groups. (1) Kasper et al. (2009) analyzed resolved near-IR (JHK) spectroscopy of the two components using Burrows et al. (2006) model atmospheres computed with ± 50 K spacing. They identified the best 3 fitting models to the data. We take the mean and RMS of their results, $T_{\text{eff},A} = 1275 \pm 25$ K and $T_{\text{eff},B} = 900 \pm 25$ K. The 25 K uncertainty is likely underestimated, as discussed in § 4.3, especially as the fit to component Ba does not appear as good as that for component Bb. (2) King et al. (2010) obtained resolved $0.6\text{--}5.0 \mu\text{m}$ spectra of the two components and compared the full spectra and the $1.25 \mu\text{m}$ K I absorption doublet to BT-Settl model atmospheres. Their comparisons applied an absolute flux calibration to the model atmospheres, based on the

¹⁰The two components of 2MASS J1209–1004AB are subject to the exact same uncertainty in the photometric distance, and we take care to track this aspect properly when drawing the Monte Carlo values. The net result is that the uncertainty of the age difference between A and B is smaller than would be expected simply from the uncertainties in the absolute ages of either component.

¹¹Table 4 indicates that 2MASS J22551861–5713056AB ($q = 0.63$), 2MASS J05185995–2828372AB ($q = 0.54$), 2MASS J12255432–2739476AB ($q = 0.63$) have comparably small mass ratios as 2MASS J1209–1004AB and ϵ Ind Bab. For these other binaries, the existing resolved measurements are insufficient to apply the isochrone test.

¹²These values agree well with the L_{bol} derived from resolved K -band photometry and our bolometric corrections in § 3.6. Using the high quality parallax to ϵ Ind A ($\pi = 276.1 \pm 0.3$ mas; van Leeuwen 2007), the K_{MKO} -band absolute magnitudes for the two components are $M_K = 13.58 \pm 0.02$ and 15.84 ± 0.03 mag, and K -band bolometric corrections are 2.87 ± 0.10 and 2.20 ± 0.10 mag (including the intrinsic scatter and the ± 0.5 subclasses uncertainty in the spectral types). Together, these give $\log(L_{\text{bol}}/L_{\odot}) = -4.67 \pm 0.04$ and -5.31 ± 0.04 dex for ϵ Ind Ba and Bb, respectively.

known luminosity and distance to the system. They found good agreement for $T_{\text{eff}} = 1300\text{--}1340$ K and $880\text{--}940$ K for the two components. We adopt the mean values and use the quoted range as the RMS.

Using the King et al. (2010) temperatures, Figure 6 shows the position of the two components of ϵ Ind Bab on the H-R diagram, and Figure 7 shows the age difference between the two components, computed in the same fashion as § 4.1. Like for 2MASS J1209–1004AB, the data are consistent with coevality for the binary, with a $\log(\text{age})$ difference of $0.5_{-0.3}^{+0.4}$ and $0.3_{-0.4}^{+0.3}$ dex from the Lyon and Tucson models, respectively, though only at the 2σ level when using the Lyon/COND models. The uncertainties are smaller for ϵ Ind Bab compared to 2MASS J1209–1004AB due to the much more precise distance and temperatures. The Kasper et al. (2009) temperatures give a similar result for the component ages, in fact slightly more consistent with coevality, though not significantly so given the uncertainties.

Our conclusion of coevality for the system agrees with the (somewhat different) approach of Kasper et al. (2009), who determine $\log(g)$ and T_{eff} by fitting model atmospheres to the resolved spectra and then use the results to compute the ages from evolutionary models. However, note that Smith et al. (2003) determine a hotter T_{eff} of 1500 ± 100 K for ϵ Ind Ba based on high resolution near-IR spectroscopy; if this temperature is adopted, then this component’s H-R diagram position is off the model loci, with an age older than 10 Gyr and inconsistent with coevality.

The age we derive from the H-R diagram is consistent with independent constraints on the age from the primary star ϵ Ind A. The most recently used estimate is $0.8\text{--}2.0$ Gyr from Lachaume et al. (1999), based on their semi-empirical relation between stellar rotational period and age. Appendix C updates the age estimate, leading to a broader range of $0.5\text{--}7.0$ Gyr. Both values for ϵ Ind A agree well with the median ages of $0.6\text{--}2.5$ Gyr derived by us from the H-R diagram analysis.

4.3. Systematic Uncertainties in T_{eff} ’s for T Dwarfs from Model Atmospheres

For both 2MASS J1209–1004AB and ϵ Ind Bab, while the models do successfully indicate that the systems are coeval, the mass information derived from the H-R diagram reveals some interesting issues. Table 5 gives the computed component masses and mass ratios, based on the same calculations used to determine the ages.

At face value, the HR diagram-derived mass ratio for 2MASS J1209–1004AB appears to be inverted, where the much brighter component A is non-sensibly indicated to be the lower-mass component. However, the formal uncertainties are very large and at the $\approx 1\sigma$ level, consistent with the $q \approx 0.5$ value inferred from evolutionary models (§ 3.7 and Table 3). For ϵ Ind Bab, the mass ratio from the H-R diagram is in good agreement with the value of $q = 0.60 \pm 0.02$ derived by McCaughrean et al. (2004), based on the component luminosities, evolutionary models, and an assumed age of $0.8\text{--}2.0$ Gyr (where we have taken the average and RMS of their computed values). So within the accuracy afforded by the current data, the mass ratios derived from the H-R diagram

seem reasonable.

However, a significant disagreement occurs when considering the total mass of ϵ Ind Bab. The total mass derived from the H-R diagram is $72_{-9}^{+10} M_{\text{Jup}}$ ($78_{-10}^{+11} M_{\text{Jup}}$) as derived from the Lyon (Tucson) models and the Kasper et al. (2009) temperatures, with the King et al. (2010) temperatures giving a slightly higher total mass of $86_{-10}^{+11} M_{\text{Jup}}$ ($95_{-12}^{+13} M_{\text{Jup}}$). (Note that the calculation of the total mass from the H-R diagram is *independent* of the aforementioned uncertainty in ϵ Ind A’s age). Such values strongly conflict with the preliminary dynamical mass of $121 \pm 1 M_{\text{Jup}}$ measured by Cardoso et al. (2009) from the binary’s relative orbital motion. And thus, there is a problem in one or more of the input data or models involved in the analysis. The observations of the component L_{bol} ’s and total dynamical mass seem secure. The L_{bol} ’s are determined by King et al. (2010) using resolved spectroscopy across a very broad wavelength range, agree well with the values obtained using near-IR photometry with our well-determined bolometric corrections (§ 4.2), and the uncertainties are fully propagated through our analysis. Likewise, the Cardoso et al. dynamical mass also seems reasonable given the large angular separation between the two components, the large number of observing epochs, and the long duration of the monitoring ($\approx 40\%$ of the derived orbital period, which should be sufficient to determine an accurate mass, e.g., as demonstrated by Bouy et al. 2004 and Dupuy et al. 2009a).

Assuming for the moment that the loci of evolutionary models are correct, this discrepancy in total mass of ϵ Ind Bab must arise from errors in the temperatures assigned to the binary components from the model atmosphere fitting.¹³ Generally speaking, changes to the relative temperatures between the two components would alter the inferred mass ratio, whereas systematic shifts to the temperatures assigned to both components would alter the derived total mass. Figures 8 and 9 summarize the changes to the HR-diagram-derived properties of the ϵ Ind Bab system (component ages, age difference, mass ratio, and total mass) if the T_{eff} ’s for the two components are changed in these three ways: relative changes in the T_{eff} ’s, overall shifts in the T_{eff} ’s, and changes to the T_{eff} of only one component. These calculations place the following constraints on the T_{eff} estimates:

- The *relative* T_{eff} difference between ϵ Ind Ba and Bb appears to be consistent with most of the constraints, namely coevality, an estimated age of ≈ 1 Gyr, and a mass ratio of ≈ 0.6 (Figure 8). However, the total mass of the system is under-predicted by the evolutionary models using these T_{eff} ’s.
- The disagreement between the total mass from the H-R diagram and the orbital monitoring

¹³A more exotic explanation would be that ϵ Ind Bab is an unresolved triple system, with one of the components being an unresolved, nearly equal-mass binary. This would increase the total mass of the system derived from the H-R diagram, since correcting for such binarity would reduce the L_{bol} of the component and lead to a higher mass for a fixed T_{eff} . However, such a change would drive the H-R diagram positions towards non-coevality (assuming the assigned T_{eff} ’s are correct). More significantly, the resolved absolute IR magnitudes of the two known components of ϵ Ind Bab are consistent with other T dwarfs of comparable spectral types (e.g., Figure 16 of Burgasser et al. 2006d), and thus correction for any unresolved binarity would make the associated component underluminous.

disappears if both components are $\approx 50\text{--}100$ K hotter (Figure 9), which still leaves the system coeval. However, an older age of ≈ 6 Gyr then results.

- Changing the T_{eff} for only one of the components cannot simultaneously fulfill the requirements of coequality and agreeing with the dynamically measured total mass (Figure 10).

Altogether, this analysis points to a small, but non-zero, systematic error of $\approx 50\text{--}100$ K in the published T_{eff} values from model atmosphere fitting. This seems plausible given the known inadequacies of the model atmospheres, especially in the L/T transition region (§ 4), and thus invoking errors in the evolutionary models is not compelling. The implied temperatures for the two components would then be $\approx 1350\text{--}1400$ K and $\approx 950\text{--}1000$ K for components Ba and Bb, respectively. For component Ba, this hotter temperature is consistent with the 1500 ± 100 K found by Smith et al. (2003) and noticeably hotter than previous fitting of early-T dwarfs ($\approx 1100\text{--}1200$ K; § 4.1). For component Bb, the implied hotter temperature agrees with that found expected for mid/late-T dwarfs based on model atmosphere fitting by Burgasser et al. (2006a), where a linear fit to their results gives 1030 K for the T6 subclass (Equation 7 of Liu et al. 2008).

The systematic T_{eff} errors that we infer from the isochrone method are comparable to the estimated uncertainties in spectral fitting of field T dwarfs (§ 4.1 and references therein), though ϵ Ind Bab provides a more stringent test of the models given this binary’s abundance of observational constraints compared to ordinary field brown dwarfs.¹⁴ Also, note that the x -axes in Figures 8– 10 show the full possible range of T_{eff} changes; larger changes would displace one or both binary components off the model loci on the H-R diagram, leading to ages that are either far too young ($\lesssim 10$ Myr) or too old ($\gtrsim 10$ Gyr).

Finally, we point out that given the measured L_{bol} ’s and dynamical mass for ϵ Ind Bab, Figure 4 shows that the evolutionary models would lead to an inferred age of about 5 Gyr. In the same fashion, King et al. (2010) have inferred an age of 3.7–4.3 Gyr from the evolutionary models (see also Cardoso et al. 2009). This is at the older end of the age range inferred for the K5V primary star ϵ Ind A (Appendix C), though the age-dating methods are largely derived for $\lesssim 1$ Gyr solar-type stars and are not well-calibrated for such old ages or for such a late-type primary. In fact, it may be that the age of the ϵ Ind ABab system is most accurately determined from brown dwarf evolutionary models, though it will be difficult to test this hypothesis independently.

¹⁴A somewhat similar, though less precise, consistency check of the atmospheric model fitting relative to the evolutionary models comes from the derived ages of field and benchmark T dwarfs, where the fitted T_{eff} and $\log(g)$ values combined with evolutionary models lead to reasonable age determinations of a few to several Gyr for single field objects (e.g. Leggett et al. 2008, 2007; Saumon et al. 2007; Burgasser et al. 2006a).

5. Conclusions

We have identified the T3 dwarf 2MASS J1209–1004 as a tight substellar binary, with an extreme mass ratio ($q \approx 0.5$) compared to previously known field brown dwarf binaries. The near-IR photometry combined with modeling of the integrated-light spectrum indicates spectral types of $T2.0 \pm 0.5$ and $T7.5 \pm 0.5$ for the two components. This newly discovered binarity lessens the utility of this object as the primary near-IR spectral-type standard for T3 dwarfs. We suggest SDSS J1206+2813 as a replacement.

The highly unequal mass ratio of the system allows us to test the joint accuracy of evolutionary and atmospheric models, by examining if the ages inferred from the H-R diagram position of the two components are consistent with coevality. Using the photometric distance to the system and latest available T_{eff} 's from model atmosphere fitting of T dwarfs, we find that the models successfully indicate that the two components of 2MASS J1209–1004AB are coeval, with a difference of $\log(\text{age}) = -0.8 \pm 1.3$ ($-1.0_{-1.3}^{+1.2}$) dex based on the Lyon (Tucson) models. A similar analysis of the T1+T6 binary ϵ Ind Bab also supports the accuracy of the models, with the system being consistent with coevality at the 1–2 σ level, depending on the choice of model atmosphere fits and evolutionary models. (The temperatures for ϵ Ind Bab from King et al. 2010 in combination with the Lyon/COND models produce the most non-coeval results, with an age difference of $\log(\text{age}) = 0.5_{-0.3}^{+0.4}$ dex.)

While the models succeed in respect to the isochrones, for ϵ Ind Bab the total mass derived from the H-R diagram ($\approx 80 M_{\text{Jup}}$) is discrepant with the measured dynamical mass of $121 \pm 1 M_{\text{Jup}}$. This is most simply resolved by assuming a systematic increase in T_{eff} for the two components by ≈ 50 –100 K warmer, i.e., an increase to ≈ 1375 K and 950 K for components Ba and Bb, respectively. Such an error is not unexpected, given the known inadequacies of the model atmospheres in the L/T transition region, the quality of the spectral fit, and the general uncertainties in the procedures used to fit such models to observed spectra. Such a T_{eff} increase leads to an implied age of about 6 Gyr for the system, somewhat older than previous estimates.

While the ≈ 50 –100 K errors are comparable to those typically cited in the atmospheric model fitting, it is worth emphasizing that ϵ Ind Bab indicates that such errors are present (i.e., non-zero), as the masses inferred from the H-R diagram are strongly discrepant with the dynamical mass, *a result that is independent of the uncertainty in the age of the system*. However, assuming the evolutionary models are basically correct, T_{eff} errors much larger than ≈ 100 K are not warranted, as the inferred properties from the H-R diagram would then be inconsistent with the underlying constraints of coevality and a mass ratio ≤ 1.0 . Also note that the very precise T_{eff} results from the T5+T5.5 mass-benchmark binary 2MASS J1534–2952AB and the M4+T8.5 age-benchmark system Wolf 940AB point to ≈ 100 K overestimates of T_{eff} when model atmospheres are used to fit the near-IR spectrum of T dwarfs (Liu et al. 2008; Burningham et al. 2009), similar in amplitude though opposite in sign to what we find here from ϵ Ind Bab. For Wolf 940B, Leggett et al. (2010a) show that luminosity-constrained model fits to the near-IR spectrum of this T8.5 dwarf are poor,

with the synthetic spectrum J and H -band peaks too high and the K -band peak too low. Most likely this is due to the known incompleteness of the molecular opacity line lists in this region.

Thus, substantial errors in evolutionary and/or atmospheric models for T dwarfs do not appear to be required, though it is not possible to fully reconcile all the model predictions with the observations, especially for ϵ Ind Bab where the measurements are exceptionally precise. It is also worth noting that Dupuy et al. (2009b) have found that the luminosities predicted by evolutionary models at ≈ 0.8 Gyr may be systematically underestimated by a factor of 2–3, based on the luminosities and dynamical masses of the L4+L4 substellar binary HD 130948BC. A simple factor of 3 boost to the model-predicted luminosities seems implausible — the model tracks on the H-R diagrams (Figure 6) would then give implausibly old ages ($\gg 10$ Gyr). Such a luminosity error could be made compatible with the H-R diagram positions if the current effective temperatures for the T dwarfs were also systematically overestimated by $\gtrsim 200$ K, but such a large discrepancy seems implausible.

Even stronger constraints on the models from the isochrone test will require smaller uncertainties in L_{bol} and T_{eff} . For 2MASS J1209–1004AB, numerical tests using the measurements from § 4.1 indicate that a $\approx 5\%$ distance and ≈ 25 K uncertainty in T_{eff} are needed to measure a 2σ discrepancy from coevality. In absence of a parallax, our analysis is consistent with coevality, but the results on absolute ages in Table 3 cannot be taken as a firm constraint. The parallax measurement is within current capabilities (e.g. Vrba et al. 2004) and is being pursued by us using the Canada-France-Hawaii Telescope (e.g. Dupuy & Liu 2009), but the required T_{eff} accuracy is a challenge to atmospheric models. Both 2MASS J1209–1004AB and ϵ Ind Bab have plausibly short orbital periods for dynamical mass determinations, which will significantly strengthen the future tests of the models. This is especially true in the case of ϵ Ind Bab, given the additional independent constraint from the age estimate of the primary star.

The immediate prospects of finding similarly extreme systems to further test the models in this fashion are limited, given that hundreds of nearby ultracool dwarfs have already been imaged at high angular resolution but yielding only 2MASS J1209–1004AB and ϵ Ind Bab. As one alternative path, Burgasser et al. (2008a) have pursued the possibility of finding previously unrecognized extreme mass-ratio ultracool binaries by modeling of integrated-light spectra, suitable for special cases where the primary and secondary spectral types are sufficiently discrepant (though the resolved measurements of the individual components needed to place them on the H-R diagram may be challenging). In the near-future, the advent of powerful new wide-field surveys, such as the Pan-STARRS optical survey (Kaiser et al. 2002) and the WISE mid-IR survey satellite (Mainzer et al. 2009), will boost the prospects for expanding the census of field brown dwarfs and thereby enable discovery of new binaries. A larger sample of extreme systems will allow the isochrone test to be applied over a wider range of temperatures and luminosities, thus challenging the models over a large span of brown dwarf masses and ages.

We gratefully acknowledge the Keck LGS AO team for their exceptional efforts in bringing

the LGS AO system to fruition. It is a pleasure to thank Jim Lyke, Hien Tran, Heather Hershley, Gary Punawai, Al Conrad, Randy Campbell, Jason McIlroy, and the Keck Observatory staff for assistance with the observations. This work has benefited from discussions with Michael Cushing, Markus Kasper, and Jon Swift. We thank David Pinfield, Nicolas Lodieu, Phillippe Delorme, Ben Burningham, and Steve Warren for providing electronic version of published late-T dwarf spectra. Our research has employed the 2MASS data products; NASA’s Astrophysical Data System; the SIMBAD database operated at CDS, Strasbourg, France; the M, L, and T dwarf compendium housed at DwarfArchives.org and maintained by Chris Gelino, Davy Kirkpatrick, and Adam Burgasser (Kirkpatrick 2003; Gelino et al. 2004); the SpeX Prism Spectral Libraries maintained by Adam Burgasser at <http://www.browndwarfs.org/spexprism>; and the VLM Binaries Archive maintained by Nick Siegler at <http://www.vlmbinaries.org>. MCL and TJD acknowledge support for this work from NSF grant AST-0507833 and an Alfred P. Sloan Research Fellowship. SKL’s research is supported by the Gemini Observatory, which is operated by the Association of Universities for Research in Astronomy, Inc., on behalf of the international Gemini partnership of Argentina, Australia, Brazil, Canada, Chile, the United Kingdom, and the United States of America. Finally, the authors wish to recognize and acknowledge the very significant cultural role and reverence that the summit of Mauna Kea has always had within the indigenous Hawaiian community. We are most fortunate to have the opportunity to conduct observations from this mountain.

Facilities: Keck II Telescope (LGS AO, NIRC2)

A. Updated Near-IR Bolometric Corrections for Ultracool Dwarfs

We improve the polynomial fit for the K -band bolometric correction as a function of near-IR spectral type from Golimowski et al. (2004a), by updating the spectral types for the T dwarfs in their sample to types from Burgasser et al. (2006b); adding data for the T dwarfs HD 3651B and HN Peg B (Liu et al. 2007; Luhman et al. 2007b; Leggett et al. 2008); and constructing fits for the J and H -band bolometric corrections. We use a 6th-order polynomial fit to accurately capture the behavior of the J and H -band data and to avoid artificially steep changes in the polynomials at the earliest and latest spectral types. The results of the new fits are shown in Figure 11 and Table 6. Note that the use of the revised spectral types for the T dwarfs leads to 30–50% smaller RMS about the fit compared to the original Golimowski et al. study.

We also plot the BC values for two of the latest type objects known, the T8.5 dwarf Wolf 940B (Burningham et al. 2009; Leggett et al. 2010a) and the T9 dwarf ULAS 0034–0052 (Warren et al. 2007; Smart et al. 2010). From the published bolometric luminosities, MKO photometry, and distances, we compute their bolometric corrections in JHK , though these are not included in the polynomial fit. The values are notably different from even the T7–T8 objects, likely due to the sharply increasing fraction of L_{bol} emitted at mid-infrared wavelengths in the very latest known objects (e.g. Figure 1 of Leggett et al. 2010b) and perhaps improvements in the methods used to derive L_{bol} for late-T dwarfs using model atmospheres since the Golimowski et al. (2004a) study,

which assumed a Rayleigh-Jeans approximation beyond $5 \mu\text{m}$.

B. Homogenous Compilation of Substellar Field Binaries

We determined or compiled from the literature the spectral types, distances, and luminosities of all ultracool field binaries with integrated-light spectral types of L4 or later or those with ancilliary evidence for being substellar. The available literature compilations are based on a broad mix of input data and calculation methods. To improve upon this, we assembled a more homogenous compilation of binary properties, as described below. The final results are in Table 4.

Photometry: For the integrated-light photometry, we preferentially used measurements on the MKO photometric system where available and 2MASS measurements for the remaining objects.

To determine the resolved photometry, we compiled the highest precision JHK flux ratio measurements available from the literature and supplemented them with measurements from public data archives (*HST*, VLT, and Gemini) and our own unpublished Keck LGS AO data. In cases where the integrated-light photometry and flux ratios were not on the same photometric system, we used conversions between MKO and 2MASS from Stephens & Leggett (2004).

Infrared data were not available for 5 binaries originally discovered by *HST* using the $F814W$ bandpass (e.g. Reid et al. 2001; Gizis et al. 2003; Bouy et al. 2003). For these cases, we estimated the K -band flux ratio from the optical results. To do this, we assumed $\Delta F814W = \Delta I$, which is accurate to ≈ 0.02 mag according to Bouy et al. (2003). To estimate the secondary’s spectral type, we derived the relation between spectral type and M_I , based on the 11 objects that were used in the Liu et al. (2006) faint relations and have I -band photometry in Dahn et al. (2002):

$$M_I = 14.83 + (6.396 \times 10^{-1}) \times \text{SpT} - (1.542 \times 10^{-2}) \times \text{SpT}^2 \quad (\text{B1})$$

where $\text{SpT} = 0$ means L0, etc, using optical spectral types for the L dwarfs. The fit is valid from L0 to T7.5, and the rms about the fit is 0.25 mag. Then using the adopted primary spectral type (described below) and the observed ΔI , we derived the secondary spectral type. With spectral types for both components, we use the Liu et al. (2006) SpT–absolute magnitude relations to estimate ΔK for the binary. We accounted for the additional uncertainty introduced by this process in our analysis, and the affected objects are marked in Table 4 as being correspondingly uncertain.

Resolved spectral types and distances: When available, we adopt the individual component spectral types previously determined from detailed analysis, e.g., spectral decomposition.

For the remaining binaries, we assumed that the primary spectral types and uncertainties were identical to the integrated-light spectral types. We adopted optical spectral types determined on the Kirkpatrick et al. (1999) classification scheme for L dwarfs and infrared types on the Burgasser et al. (2006b) classification scheme for T dwarfs, except in two cases. One was

DENIS-P J225210.7–173013AB, which Kendall et al. (2004) classified as L7.5 based on a comparison of the H and K -band spectra to those of optically typed L dwarfs. The other was 2MASS J09201223+3517429AB, which has highly discrepant integrated-light spectral types of L6.5 in the optical (Kirkpatrick et al. 2000) and T0p in the infrared. We adopted the infrared type in this case.

To derive the secondary spectral types, we used the average of the “faint” and “bright” SpT–absolute magnitude relations of Liu et al. (2006) along with the known or estimated absolute magnitudes for the secondaries. (The Liu et al. relations were extended to objects of M6–L1 using photometry from the Leggett et al. 2010b literature compilation.) For binaries with parallax measurements, we computed the absolute magnitudes of the secondary components directly. For the rest, we estimated photometric distances based on the primary components’ apparent magnitudes and the same averaged Liu et al. (2006) SpT–absolute magnitude relations. If distance estimates were available from multiple bandpasses, we preferred the K -band estimate, then H -band, and finally J -band, to minimize the potential non-monotonic behavior in the L/T transition region. The uncertainties in the resulting distances account for the input photometry uncertainties and the intrinsic scatter in the empirical relations.

Using the final assembled IR absolute magnitudes for the secondaries, we estimated spectral types using the method described in Section 3.2 of Dupuy et al. (2009c). For a given bandpass, we computed the spectral type probability distribution for an object based on its absolute magnitude, the uncertainties in both the photometry and the distances, and the intrinsic scatter in the empirical SpT–absolute magnitude relations. We then combined the results from all available bandpasses to form the joint spectral type probability distribution and thus to estimate the final secondary spectral types and uncertainties. We rounded all spectral types and their uncertainties to the nearest 0.5 subclass.

Bolometric luminosities and luminosity ratios: We derived individual luminosities for the binary components from each available bandpass (JHK) using the resolved photometry, distances, and bolometric corrections. Bolometric corrections were computed based on the polynomial fits in Appendix A and the spectral types assigned to each component. For computing luminosities, we assume $M_{\text{bol},\odot} = 4.75$ mag. Uncertainties for the resulting L_{bol} ’s were computed from the uncertainties in the resolved photometry, in the bolometric corrections due to the spectral type errors, and the intrinsic scatter in the bolometric correction relations.

We also computed luminosity ratios for each available bandpass; this is typically known to higher precision than L_{bol} since the ratios are independent of the distance uncertainty. The error in the luminosity ratio comes from the quadrature sum of the errors in the flux ratios and the bolometric corrections of the primaries and secondaries. For our final adopted luminosities and luminosity ratios, we chose the bandpass that gave the smallest error in the luminosity ratio.

Mass ratios: We used the Burrows et al. (1997) evolutionary models to derive the mass ratios for

each system, using the derived L_{bol} 's, their uncertainties, and an adopted age. We take care to treat the distance uncertainty as an error common to each binary, as opposed to applying it independently to each individual component. For objects with specific age information in the literature, we use that; otherwise we assume 1 Gyr. In both cases, we ignore the age uncertainty in calculating the mass ratio, since this is common to (most of) the objects. Four binaries have their total mass measured dynamically, and we use their published mass ratio measurements in these cases: 2MASS J1534–2952AB (Liu et al. 2008), HD 130948BC (Dupuy et al. 2009b), LP 349–25AB, and GJ 569Bab (Dupuy et al. 2010).

To summarize the mass ratio results, we fit the observed values with a power-law distribution.¹⁵ Since the sample is relatively sparse, instead of the usual process of fitting to a binned histogram, we adopt a maximum likelihood approach. The probability distribution of the mass ratio q is described by

$$P(q) = (\alpha + 1) q^\alpha \quad (\text{B2})$$

for $q = 0 - 1$, with the constant chosen so that the total probability is unity. We define the log of the likelihood function as

$$\mathcal{L} \equiv \ln P(q|\alpha) = \ln \prod_{i=1}^n (\alpha + 1) q_i^\alpha \quad (\text{B3})$$

$$= \sum_{i=1}^n \left[\ln(\alpha + 1) + \alpha \ln q_i \right] \quad (\text{B4})$$

$$= n \ln(\alpha + 1) + \alpha \sum_{i=1}^n \ln q_i \quad (\text{B5})$$

where n is the number of objects in the sample and q_i is the mass ratio for each object. To find the best fitting α , we find the maximum of \mathcal{L} :

$$\frac{d\mathcal{L}}{d\alpha} = \frac{n}{\alpha + 1} + \sum_{i=1}^n \ln q_i = 0 \quad (\text{B6})$$

which gives the final result

$$\alpha = - \left[1 + \frac{n}{\sum_{i=1}^n \ln q_i} \right]. \quad (\text{B7})$$

For our sample, the distribution $\mathcal{L}(\alpha)$ is well-fit by a gaussian, from which we extract 1σ confidence limits. To incorporate the uncertainties in q_i , we use a Monte Carlo approach, computing the best

¹⁵We exclude the L6p+T7.5p system, SDSS J141624.08+134826.7AB, from this ensemble analysis given its unusually large separation and mass ratio compared to all other field systems. Also, because of its large L_{bol} ratio, its mass ratio estimate is highly dependent on the assumed age, from 0.2 to 0.5 for ages of 1 to 10 Gyr.

α many times with the q_i values drawn from normal distributions; the resulting RMS dispersion in α from the ensemble of results is much smaller than the 68% confidence interval in any realization of \mathcal{L} . As a simple approximation, we add the RMS ($\sigma_\alpha = 0.3$) in quadrature to the confidence limits ($\sigma_\alpha = 0.6$) to obtain our final uncertainty on α .

We find $\alpha = 4.9 \pm 0.7$ for the sample in Table 4. For such an exponent, binaries with $q \leq 0.65$ such as ϵ Ind Bab and 2MASS J1209–1004AB amount to only 9% of the population. Our result is comparable to, though somewhat steeper, than the $q^{(4.2 \pm 1.0)}$ found by Burgasser et al. (2006d) for a sample of 30 binaries with estimated primary masses of $<0.075 M_\odot$. There are some differences in the fitting method and the input data; for the latter, the Burgasser et al. compilation included young binaries in open clusters and star-forming regions (which tend to have a broader range of mass ratios) and used the heterogenous set of mass ratios published in the literature. Burgasser et al. also corrected the observed mass ratio distribution to account for the bias towards equal-mass systems in magnitude-limited surveys, based on an approximate conversion between flux ratio and mass ratio (see Burgasser et al. 2003). We choose not to apply any corrections, since the surveys involved in Table 4 span a wide range of wavelengths and telescopes. Given these differences, a more shallow power-law is expected from the Burgasser et al. compilation. Similarly, using a full Bayesian analysis to account for differing survey sensitivities, Allen (2007) derived $\alpha = 1.8 \pm 0.6$; his sample included many late-M (stellar) primaries which likely led to a shallower exponent.

C. Summary of Age Estimates for ϵ Ind A

Age determinations for the K5V star ϵ Ind A are necessarily indirect and rely on empirical correlations between stellar activity, rotation, and age. Lachaume et al. (1999) estimated a mean $\log(\text{age}) = 9.1$ (1.3 Gyr) with a range of 8.9 – 9.3 (0.8 – 2.0 Gyr), based on their semi-empirical relation between stellar rotational period and age and the *estimated* rotational period of ϵ Ind A from Saar & Osten (1997) as derived from Ca II measurements and an empirical relation between chromospheric activity and rotation. This age range has been used for analysis of ϵ Ind Bab in previous work (e.g. Kasper et al. 2009; McCaughrean et al. 2004; Scholz et al. 2003).

Additional age estimates come from the correlation between age and chromospheric activity traced by Ca II line emission, as measured by the R'_{HK} index. Henry et al. (1996) measured ϵ Ind A on three occasions spanning 1.3 yr, with a mean and an rms of $\log R'_{HK} = -4.56 \pm 0.01$ dex. Chromospheric activity is known to be variable on decade-long time scales, and Gray et al. (2006) found $\log R'_{HK} = -4.85$ for ϵ Ind roughly eight years later.

The available age calibrations of R'_{HK} give consistent estimates. (1) Using the Donahue (1998) calibration, we find ages of 1.2 Gyr and 3.2 Gyr from the Henry et al. (1996) and Gray et al. (2006) data, respectively. (2) The Soderblom et al. (1991) calibration results in ages of 1.2 Gyr and 3.4 Gyr. (3) Note that with a $B - V$ color of 1.06 mag (Perryman et al. 1997), ϵ Ind A is beyond the most recent activity-age calibrations, those of Mamajek & Hillenbrand (2008) which are only valid for

$0.5 < B - V < 0.9$ mag stars. If we disregard this limitation, their R'_{HK} calibration gives ages of 0.9 and 4.0 Gyr for the two sets of measurements. (4) We can also use the “preferred” method of Mamajek & Hillenbrand (2008), namely converting R'_{HK} to a Rossby number, in order to estimate a rotation period that can then be used to derive an age from their gyrochronology relation. The resulting ages are 1.6 Gyr and 5.0 Gyr for the higher and lower activity levels, respectively. The nominal uncertainty for such chromospheric ages is estimated to be around $\pm 50\%$ at a single epoch (Soderblom et al. 1991; Mamajek & Hillenbrand 2008). Thus, the overall age range derived from chromospheric indicators is 0.5–7.0 Gyr, with a mean of about 2 Gyr.

An alternative estimate comes from Janson et al. (2009). They obtained high-contrast imaging of the system to attempt to directly image a close-in substellar companion, whose existence has been inferred from a long-term linear trend in the radial velocity of ϵ Ind A (Endl et al. 2002). By combining their imaging non-detection combined with the radial velocity data, Janson et al. conclude that the star is likely to be older than ≈ 1 Gyr, or else the companion would have been sufficiently self-luminous to have been directly detected.

This age estimate may be improved in the future by measuring ϵ Ind A’s rotation period, as gyrochronology relations can provide more precise age estimates (15–25%; Barnes 2007).¹⁶ Based on Mamajek & Hillenbrand (2008), the rotation period of ϵ Ind A is expected to be 14–50 days given its level of chromospheric activity. Furthermore, because ϵ Ind A is a very bright star ($V = 4.7$ mag), it is within reach of asteroseismological measurements with current facilities, which may be able to provide an even more precise age estimate.

REFERENCES

- Adams, T., Davies, M. B., Jameson, R. F., & Scally, A. 2002, MNRAS, 333, 547
- Allen, P. R. 2007, ApJ, 668, 492
- Allers, K. N., Liu, M. C., Dupuy, T. J., & Cushing, M. C. 2010, ApJ, in press
- Baraffe, I., Chabrier, G., Barman, T. S., Allard, F., & Hauschildt, P. H. 2003, A&A, 402, 701
- Baraffe, I., Chabrier, G., & Gallardo, J. 2009, ApJ, 702, L27
- Barnes, S. A. 2007, ApJ, 669, 1167
- Bouvier, J., et al. 2008, A&A, 481, 661
- Bouy, H., Brandner, W., Martín, E. L., Delfosse, X., Allard, F., & Basri, G. 2003, AJ, 126, 1526

¹⁶Using the aforementioned Saar & Osten (1997) rotation period estimate, Barnes (2007) compute a gyrochronological age of 1.03 ± 0.13 Gyr for ϵ Ind A. This age should be considered notional, since it relies on an estimated period, not a direct measurement.

- Bouy, H., et al. 2004, *A&A*, 423, 341
- . 2008, *A&A*, 481, 757
- Bowler, B. P., Liu, M. C., & Dupuy, T. J. 2010, *ApJ*, 710, 45
- Burgasser, A. J. 2007, *ApJ*, 659, 655
- Burgasser, A. J., Burrows, A., & Kirkpatrick, J. D. 2006a, *ApJ*, 639, 1095
- Burgasser, A. J., Cruz, K. L., Cushing, M., Gelino, C. R.,Looper, D. L., Faherty, J. K., Kirkpatrick, J. D., & Reid, I. N. 2010a, *ApJ*, 710, 1142
- Burgasser, A. J., Geballe, T. R., Leggett, S. K., Kirkpatrick, J. D., & Golimowski, D. A. 2006b, *ApJ*, 637
- . 2006c, *ApJ*, 637, 1067
- Burgasser, A. J., Kirkpatrick, J. D., Cruz, K. L., Reid, I. N., Leggett, S. K., Liebert, J., Burrows, A., & Brown, M. E. 2006d, *ApJS*, 166, 585
- Burgasser, A. J., Kirkpatrick, J. D., & Lowrance, P. J. 2005a, *AJ*, 129, 2849
- Burgasser, A. J., Kirkpatrick, J. D., Reid, I. N., Brown, M. E., Miskay, C. L., & Gizis, J. E. 2003, *ApJ*, 586, 512
- Burgasser, A. J., Liu, M. C., Ireland, M. J., Cruz, K. L., & Dupuy, T. J. 2008a, *ApJ*, 681, 579
- Burgasser, A. J.,Looper, D., & Rayner, J. T. 2010b, *AJ*, 139, 2448
- Burgasser, A. J., McElwain, M. W., Kirkpatrick, J. D., Cruz, K. L., Tinney, C. G., & Reid, I. N. 2004, *AJ*, 127, 2856
- Burgasser, A. J., Reid, I. N., Leggett, S. K., Kirkpatrick, J. D., Liebert, J., & Burrows, A. 2005b, *ApJ*, 634, L177
- . 2005c, *ApJ*, 634, L177
- Burgasser, A. J., Reid, I. N., Siegler, N., Close, L., Allen, P., Lowrance, P., & Gizis, J. 2007, in *Protostars and Planets V*, ed. B. Reipurth, D. Jewitt, & K. Keil, 427–441
- Burgasser, A. J., Tinney, C. G., Cushing, M. C., Saumon, D., Marley, M. S., Bennett, C. S., & Kirkpatrick, J. D. 2008b, *ApJ*, 689, L53
- Burgasser, A. J., et al. 2000, *ApJ*, 531, L57
- . 2002, *ApJ*, 564, 421
- Burningham, B., et al. 2008, *MNRAS*, 391, 320

- . 2009, MNRAS, 395, 1237
- . 2010, MNRAS, 404, 1952
- Burrows, A., Sudarsky, D., & Hubeny, I. 2006, ApJ, 640, 1063
- Burrows, A., et al. 1997, ApJ, 491, 856
- Cardoso, C. V., et al. 2009, in American Institute of Physics Conference Series, Vol. 1094, American Institute of Physics Conference Series, ed. E. Stempels, 509–512
- Chabrier, G., Baraffe, I., Allard, F., & Hauschildt, P. 2000, ApJ, 542, 464
- Chiu, K., et al. 2008, MNRAS, 385, L53
- . 2006, AJ, 131, 2722
- Cruz, K. L., Kirkpatrick, J. D., & Burgasser, A. J. 2009, AJ, 137, 3345
- Cruz, K. L., et al. 2007, AJ, 133, 439
- Cushing, M. C., et al. 2008, ApJ, 678, 1372
- Cutri, R. M., et al. 2003, 2MASS All Sky Catalog of Point Sources.
- Dahn, C. C., et al. 2002, AJ, 124, 1170
- Delorme, P., et al. 2008, A&A, 482, 961
- Donahue, R. A. 1998, in ASP Conf. Ser. 154: Cool Stars, Stellar Systems, and the Sun, Vol. 10, 1235
- Dupuy, T., Liu, M., Bowler, B., Cushing, M., Helling, C., Witte, S., & Hauschildt, P. 2010, ArXiv e-prints
- Dupuy, T. J., & Liu, M. C. 2009, in Bulletin of the American Astronomical Society, Vol. 41, Bulletin of the American Astronomical Society, 201
- Dupuy, T. J., Liu, M. C., & Bowler, B. P. 2009a, ArXiv e-prints
- Dupuy, T. J., Liu, M. C., & Ireland, M. J. 2009b, ApJ, 692, 729
- . 2009c, ApJ, 699, 168
- Endl, M., Kürster, M., Els, S., Hatzes, A. P., Cochran, W. D., Dennerl, K., & Döbereiner, S. 2002, A&A, 392, 671
- Faherty, J. K., Burgasser, A. J., West, A. A., Bochanski, J. J., Cruz, K. L., Shara, M. M., & Walter, F. M. 2010, AJ, 139, 176

- Forveille, T., et al. 2005, *A&A*, 435, L5
- Gatewood, G., & Coban, L. 2009, *AJ*, 137, 402
- Geballe, T., et al. 2002, *ApJ*, 564, 466
- Gelino, C. R., Kirkpatrick, J. D., & Burgasser, A. J. 2004, *BAAS*, 205
- Ghez, A. M., et al. 2008, *ApJ*, 689, 1044
- Gizis, J. E., Monet, D. G., Reid, I. N., Kirkpatrick, J. D., Liebert, J., & Williams, R. J. 2000, *AJ*, 120, 1085
- Gizis, J. E., Reid, I. N., Knapp, G. R., Liebert, J., Kirkpatrick, J. D., Koerner, D. W., & Burgasser, A. J. 2003, *AJ*, 125, 3302
- Golimowski, D. A., et al. 2004a, *AJ*, 127, 3516
- . 2004b, *AJ*, 128, 1733
- Goto, M., et al. 2002, *ApJ*, 567, L59
- Gray, R. O., Corbally, C. J., Garrison, R. F., McFadden, M. T., Bubar, E. J., McGahee, C. E., O’Donoghue, A. A., & Knox, E. R. 2006, *AJ*, 132, 161
- Hartigan, P., Strom, K. M., & Strom, S. E. 1994, *ApJ*, 427, 961
- Hawley, S. L., et al. 2002, *AJ*, 123, 3409
- Henry, T. J., Jao, W., Subasavage, J. P., Beaulieu, T. D., Ianna, P. A., Costa, E., & Méndez, R. A. 2006, *AJ*, 132, 2360
- Henry, T. J., & Kirkpatrick, J. D. 1990, *ApJ*, 354, L29
- Henry, T. J., Soderblom, D. R., Donahue, R. A., & Baliunas, S. L. 1996, *AJ*, 111, 439
- Ireland, M. J., Kraus, A., Martinache, F., Lloyd, J. P., & Tuthill, P. G. 2008, *ApJ*, 678, 463
- Janson, M., et al. 2009, *MNRAS*, 399, 377
- Kaiser, N., et al. 2002, in *Survey and Other Telescope Technologies and Discoveries*. Edited by Tyson, J. Anthony; Wolff, Sidney. *Proc. of the SPIE*, Volume 4836, pp. 154-164 (2002)., 154–164
- Kasper, M., Burrows, A., & Brandner, W. 2009, *ApJ*, 695, 788
- Kendall, T. R., Delfosse, X., Martín, E. L., & Forveille, T. 2004, *A&A*, 416, L17
- King, R. R., McCaughrean, M. J., Homeier, D., Allard, F., Scholz, R., & Lodieu, N. 2010, *A&A*, 510, A99+

- Kirkpatrick, J. D. 2003, in Proceedings of IAU Symposium 211: Brown Dwarfs, ed. E. Martin, 189
- Kirkpatrick, J. D., Dahn, C. C., Monet, D. G., Reid, I. N., Gizis, J. E., Liebert, J., & Burgasser, A. J. 2001, *AJ*, 121, 3235
- Kirkpatrick, J. D., et al. 1999, *ApJ*, 519, 802
- . 2000, *AJ*, 120, 447
- Knapp, G. R., et al. 2004, *AJ*, 127, 3553
- Koerner, D. W., Kirkpatrick, J. D., McElwain, M. W., & Bonaventura, N. R. 1999, *ApJ*, 526, L25
- Konopacky, Q. M., Ghez, A. M., Barman, T. S., Rice, E. L., Bailey, J. I., White, R. J., McLean, I. S., & Duchêne, G. 2010, *ApJ*, in press (arXiv:1001.4800)
- Kraus, A. L., & Hillenbrand, L. A. 2009, *ApJ*, 704, 531
- Lachaume, R., Dominik, C., Lanz, T., & Habing, H. J. 1999, *A&A*, 348, 897
- Lane, B. F., Zapatero Osorio, M. R., Britton, M. C., Martín, E. L., & Kulkarni, S. R. 2001, *ApJ*, 560, 390
- Leggett, S. K., Hauschildt, P. H., Allard, F., Geballe, T. R., & Baron, E. 2002a, *MNRAS*, 332, 78
- Leggett, S. K., Marley, M. S., Freedman, R., Saumon, D., Liu, M. C., Geballe, T. R., Golimowski, D. A., & Stephens, D. C. 2007, *ArXiv e-prints*, 705
- Leggett, S. K., et al. 2008, *ApJ*, 682, 1256
- Leggett, S. K., Saumon, D., Burningham, B., Cushing, M. C., Marley, M. S., & Pinfield, D. J. 2010a, *ArXiv e-prints*
- Leggett, S. K., et al. 2000, *ApJ*, 536, L35
- . 2002b, *ApJ*, 564, 452
- . 2010b, *ApJ*, 710, 1627
- Liu, M. C., Dupuy, T. J., & Ireland, M. J. 2008, *ApJ*, 689, 436
- Liu, M. C., & Leggett, S. K. 2005, *ApJ*, 634, 616
- Liu, M. C., Leggett, S. K., & Chiu, K. 2007, *ApJ*, 660, 1507
- Liu, M. C., Leggett, S. K., Golimowski, D. A., Chiu, K., Fan, X., Geballe, T. R., Schneider, D. P., & Brinkmann, J. 2006, *ApJ*, 647, 1393
- Lodieu, N., Dobbie, P. D., Deacon, N. R., Hodgkin, S. T., Hambly, N. C., & Jameson, R. F. 2007, *MNRAS*, 380, 712

- Looper, D. L., Gelino, C. R., Burgasser, A. J., & Kirkpatrick, J. D. 2008, *ApJ*, 685, 1183
- Looper, D. L., Kirkpatrick, J. D., & Burgasser, A. J. 2007, *AJ*, 134, 1162
- Luhman, K. L. 1999, *ApJ*, 525, 466
- Luhman, K. L., Joergens, V., Lada, C., Muzerolle, J., Pascucci, I., & White, R. 2007a, in *Protostars and Planets V*, ed. B. Reipurth, D. Jewitt, & K. Keil, 443–457
- Luhman, K. L., et al. 2007b, *ApJ*, 654, 570
- Mainzer, A. K., Kirkpatrick, D., Wright, E., Padgett, D., & McLean, I. 2009, in *Bulletin of the American Astronomical Society*, Vol. 41, *Bulletin of the American Astronomical Society*, 365
- Mamajek, E. E., & Hillenbrand, L. A. 2008, *ApJ*, 687, 1264
- Martín, E. L., Brandner, W., & Basri, G. 1999, *Science*, 283, 1718
- Martín, E. L., Brandner, W., Bouy, H., Basri, G., Davis, J., Deshpande, R., & Montgomery, M. M. 2006, *A&A*, 456, 253
- Martín, E. L., Koresko, C. D., Kulkarni, S. R., Lane, B. F., & Wizinowich, P. L. 2000, *ApJ*, 529, L37
- McCaughrean, M. J., Close, L. M., Scholz, R.-D., Lenzen, R., Biller, B., Brandner, W., Hartung, M., & Lodieu, N. 2004, *A&A*, 413, 1029
- Monet, D. G., et al. 2003, *AJ*, 125, 984
- Perryman, M. A. C., et al. 1997, *A&A*, 323, L49
- Pinfield, D. J., et al. 2008, *MNRAS*, 390, 304
- Potter, D., Martín, E. L., Cushing, M. C., Baudoz, P., Brandner, W., Guyon, O., & Neuhäuser, R. 2002, *ApJ*, 567, L133
- Reid, I. N., Gizis, J. E., Kirkpatrick, J. D., & Koerner, D. W. 2001, *AJ*, 121, 489
- Reid, I. N., Lewitus, E., Allen, P. R., Cruz, K. L., & Burgasser, A. J. 2006a, *AJ*, 132, 891
- Reid, I. N., Lewitus, E., Burgasser, A. J., & Cruz, K. L. 2006b, *ApJ*, 639, 1114
- Reid, I. N., et al. 2008, *AJ*, 136, 1290
- Reiners, A. 2009, *ApJ*, 702, L119
- Reiners, A., Seifahrt, A., & Dreizler, S. 2010, *A&A*, 513, L9+
- Saar, S. H., & Osten, R. A. 1997, *MNRAS*, 284, 803

- Saumon, D., Geballe, T. R., Leggett, S. K., Marley, M. S., Freedman, R. S., Lodders, K., Fegley, Jr., B., & Sengupta, S. K. 2000, *ApJ*, 541, 374
- Saumon, D., Marley, M. S., Cushing, M. C., Leggett, S. K., Roellig, T. L., Lodders, K., & Freedman, R. S. 2006, *ApJ*, 647, 552
- Saumon, D., et al. 2007, *ApJ*, 656, 1136
- Schaefer, G. H., Simon, M., Prato, L., & Barman, T. 2008, *AJ*, 135, 1659
- Scholz, R. 2010, *A&A*, 510, L8+
- Scholz, R.-D., McCaughrean, M. J., Lodieu, N., & Kuhlbrodt, B. 2003, *A&A*, 398, L29
- Siegler, N., Close, L. M., Burgasser, A. J., Cruz, K. L., Marois, C., Macintosh, B., & Barman, T. 2007, *AJ*, 133, 2320
- Smart, R. L., et al. 2010, *A&A*, 511, A30+
- Smith, V. V., et al. 2003, *ApJ*, 599, L107
- Soderblom, D. R., Duncan, D. K., & Johnson, D. R. H. 1991, *ApJ*, 375, 722
- Stephens, D. C., & Leggett, S. K. 2004, *PASP*, 116, 9
- Stephens, D. C., et al. 2009, *ApJ*, 702, 154
- Stumpf, M. B., Brandner, W., Bouy, H., Henning, T., & Hippler, S. 2010, *A&A*, 516, A37+
- Tinney, C. G., Burgasser, A. J., & Kirkpatrick, J. D. 2003, *AJ*, 126, 975
- Tinney, C. G., Burgasser, A. J., Kirkpatrick, J. D., & McElwain, M. W. 2005, *AJ*, 130, 2326
- Torres, G. 1999, *PASP*, 111, 169
- van Dam, M. A., et al. 2006, *PASP*, 118, 310
- van Leeuwen, F. 2007, *A&A*, 474, 653
- Vrba, F. J., et al. 2004, *AJ*, 127, 2948
- Warren, S. J., et al. 2007, *MNRAS*, 381, 1400
- White, R. J., Ghez, A. M., Reid, I. N., & Schultz, G. 1999, *ApJ*, 520, 811
- Wilson, J. C., Kirkpatrick, J. D., Gizis, J. E., Skrutskie, M. F., Monet, D. G., & Houck, J. R. 2001, *AJ*, 122, 1989
- Wizinowich, P. L., et al. 2006, *PASP*, 118, 297

Zapatero Osorio, M. R., Lane, B. F., Pavlenko, Y., Martín, E. L., Britton, M., & Kulkarni, S. R.
2004, ApJ, 615, 958

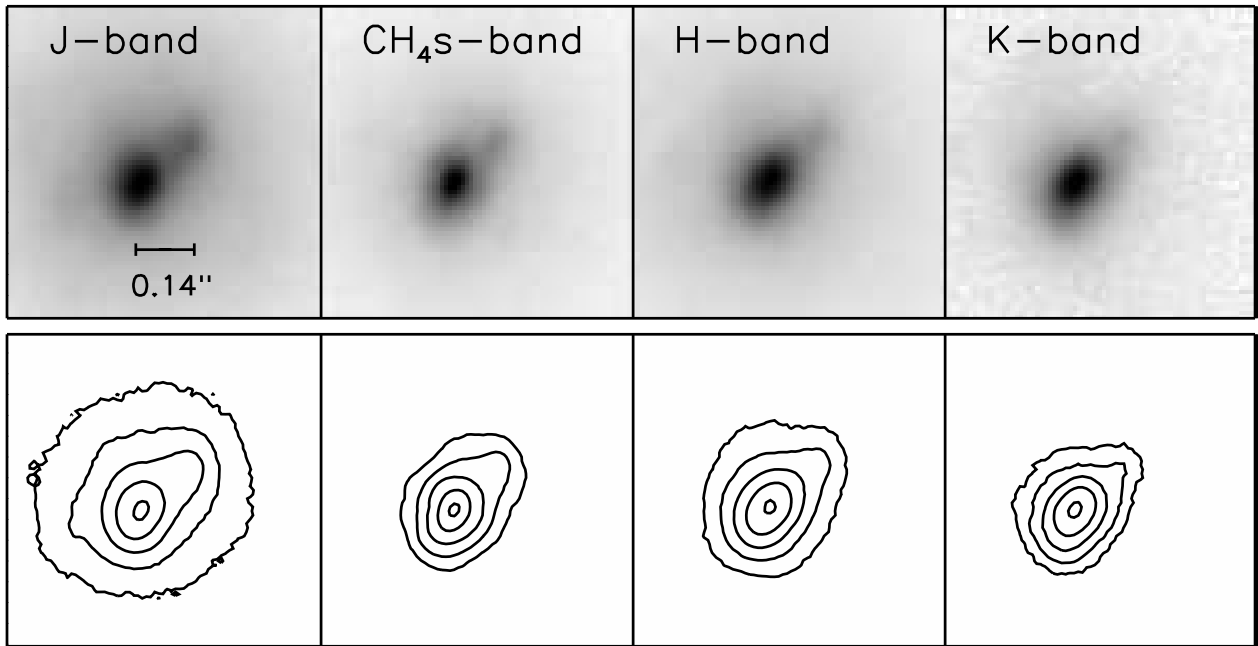


Fig. 1.— Keck LGS AO imaging of 2MASS J1209–1004AB. North is up and east is left. Each image is $0.75''$ on a side. Contours are drawn from 90%, 45%, 22.5%, 11.2%, and 5.6% of the peak value in each bandpass.

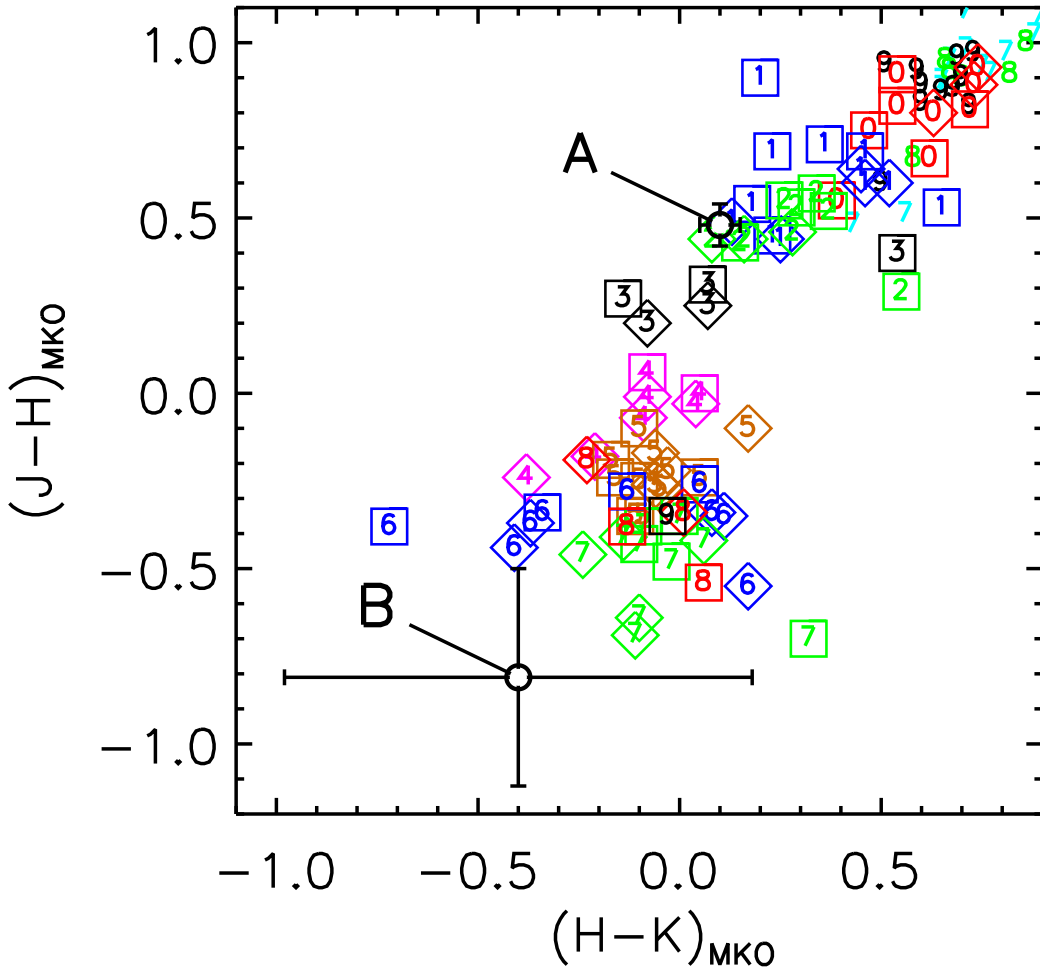


Fig. 2.— Resolved near-IR colors of the components of 2MASS J1209–1004AB compared with single late-L and T dwarfs from Knapp et al. (2004) and Chiu et al. (2006); late-T dwarfs ($\geq T6$) from Warren et al. (2007), Chiu et al. (2008), Pinfield et al. (2008), Delorme et al. (2008), and Burningham et al. (2008); and individual components of resolved binaries from McCaughrean et al. (2004), Burgasser et al. (2005b), Burgasser et al. (2006d), Liu & Leggett (2005), and Liu et al. (2006). (For the T8.5 dwarf CFBDS 0059–0114, the K -band measurement is synthesized from the near-IR spectrum and K_S -band photometry of Delorme et al. 2008.) The photometry errors are comparable to or smaller than the size of the plotting symbols for most of the objects. The numbers indicate the near-IR spectral subclass of the objects, with half subclasses being rounded down (e.g., T3.5 is labeled as “3”), and objects of the same subclass plotted in the same color. The late-L dwarfs (classified on the Geballe et al. 2002 scheme) are plotted as bare numbers. The T dwarfs (on the Burgasser et al. 2006b scheme with extension by Burningham et al. 2008) are plotted as circumscribed numbers, with squares for integer subclasses (e.g., T3) and diamonds for half subclasses (e.g., T3.5).

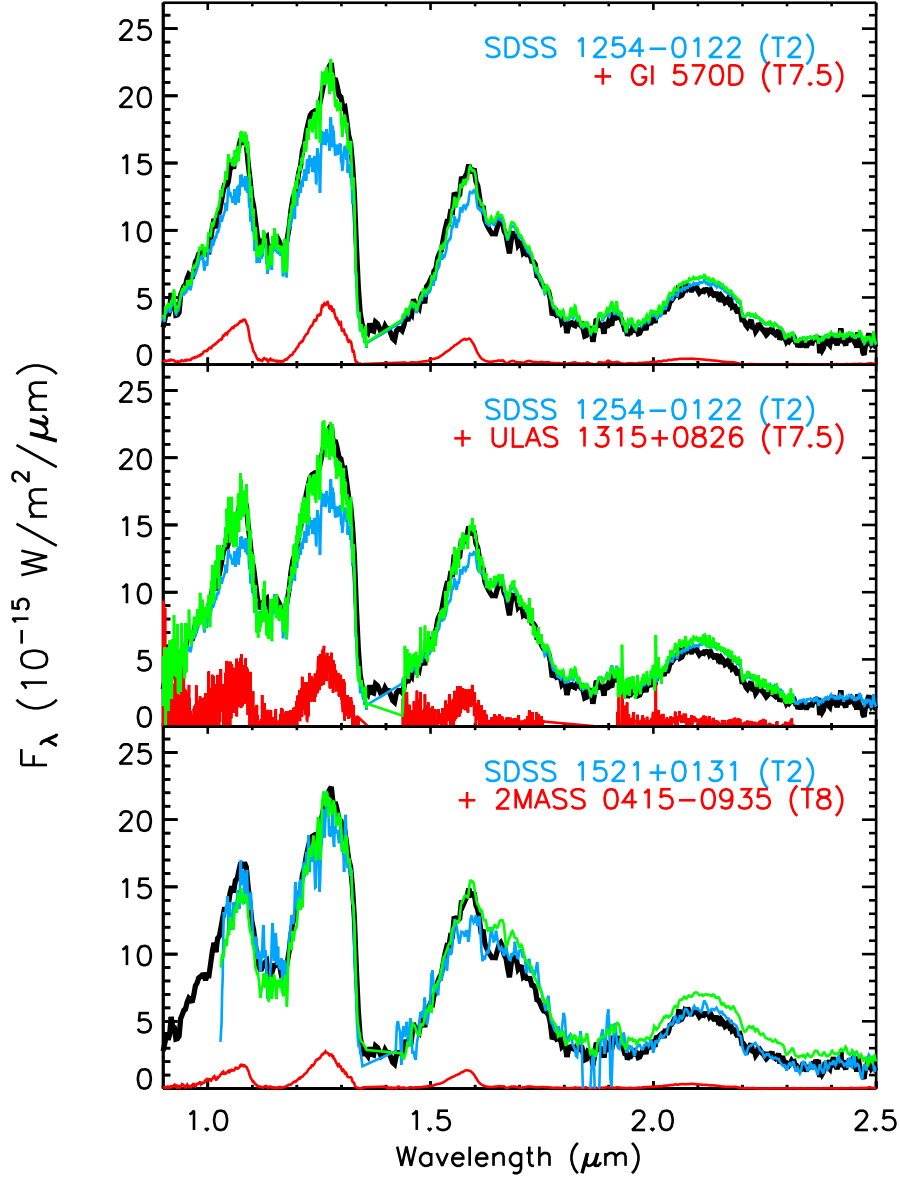


Fig. 3.— The integrated-light near-IR spectrum of 2MASS J1209–1004AB (heavy black line; Burgasser et al. 2004) modeled as the sum of two T dwarfs (green lines): one early-T template (blue lines) and one late-T template (red lines). The templates are chosen based on their similar JHK colors to the two components of 2MASS J1209–1004AB. The agreement between the observed spectrum and the modeled blends is good, meaning that the spectral types inferred for 2MASS J1209–1004A and B from the near-IR photometry are consistent with the integrated-light spectrum.

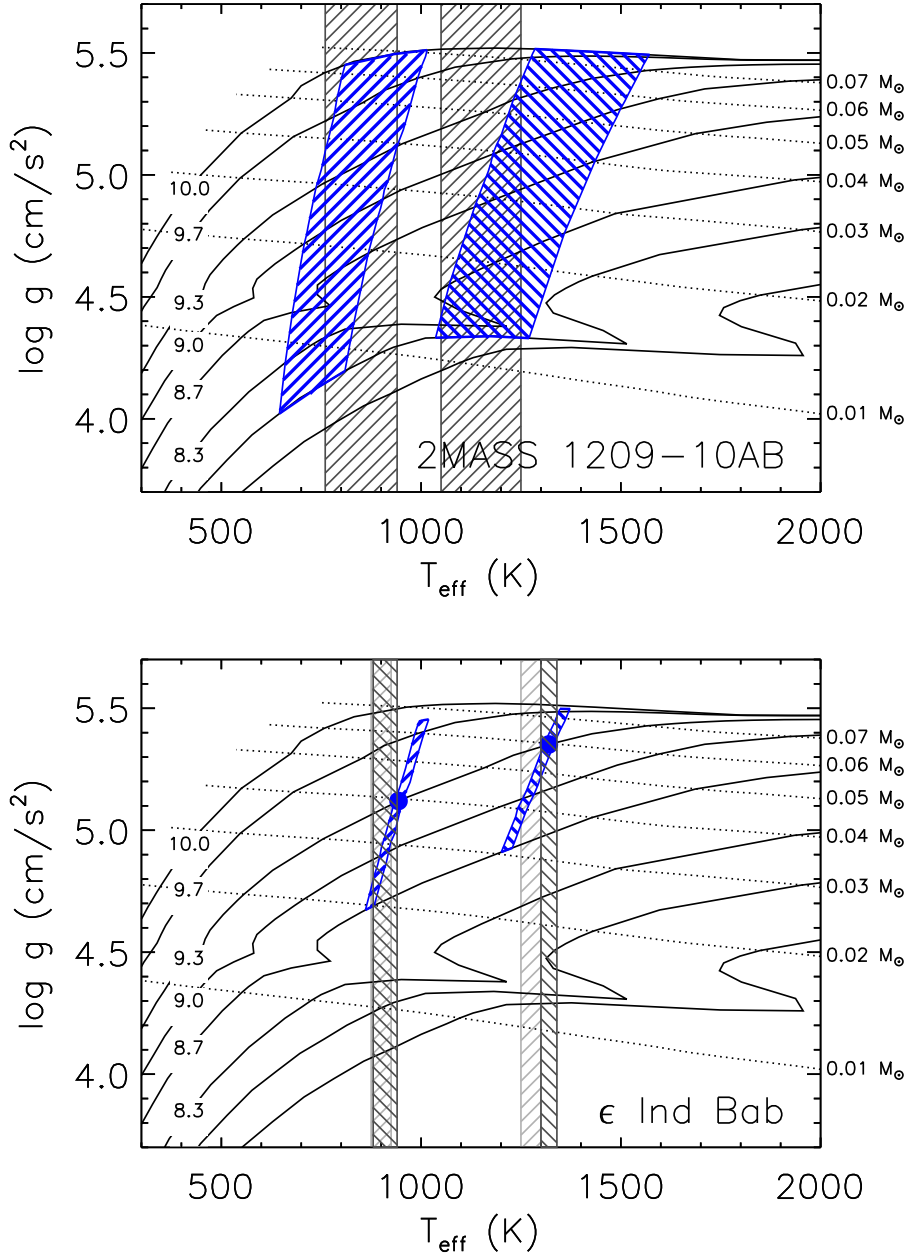


Fig. 4.— Inferred T_{eff} and $\log(g)$ for the components of 2MASS J1209–1004AB and ϵ Ind Bab based on solar-metallicity evolutionary models by Burrows et al. (1997). The blue-colored hatched regions show the constraints from the observed L_{bol} 's of the binary components and the inferred system ages, with the A component for each system being the region on the right (i.e., the hotter object). For 2MASS J1209–1004AB, we plot a generic age range of 0.1–10 Gyr. For ϵ Ind Bab, we plot an age range of 0.5–7.0 Gyr, with the filled circle representing 2 Gyr. The uncertain L_{bol} 's of 2MASS J1209–1004AB are reflected in its relatively wide hatched regions; these can be improved with a parallax determination for the system. The solid lines are isochrones from 0.1 to 10 Gyr, labeled by the logarithm of their age; the two unlabeled isochrones are 0.05 and 0.1 Gyr. Dotted lines represent iso-mass models, labeled on the right of the plot in units of M_{\odot} . The vertical grey regions show the T_{eff} 's for the two components derived from model atmosphere fitting; for ϵ Ind Bab, we show the T_{eff} values from both Kasper et al. (2009) (cooler values, in light grey) and King et al. (2010) (hotter values, in dark grey).

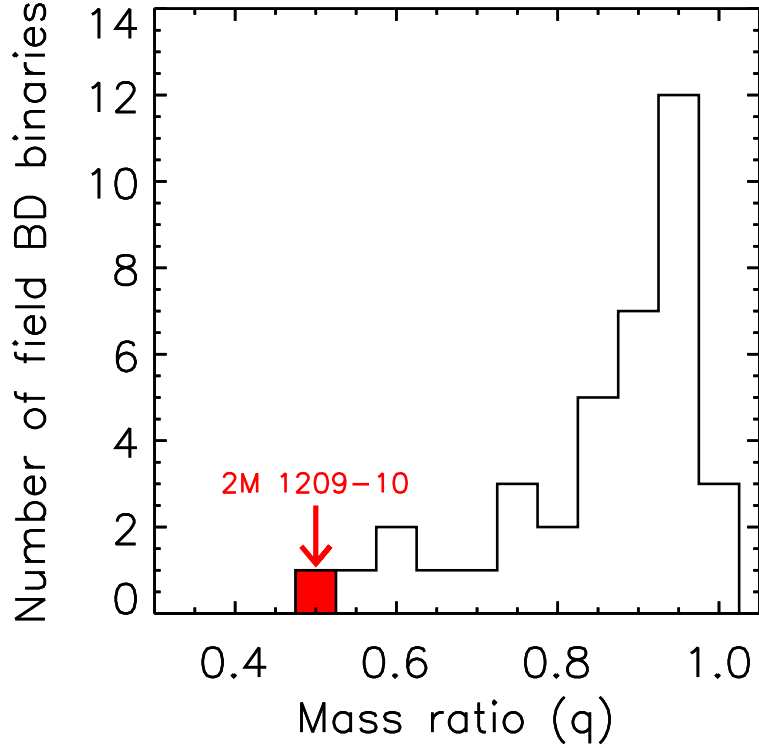


Fig. 5.— Mass ratios for all known field brown dwarf binaries, based on our compilation given in Table 4 and described in Appendix B. The mass ratio for 2MASS J1209–1004AB from our calculations is shown as the filled color bar, demonstrating the rarity of such an unequal mass ratio among the field population. (SDSS J141624.08+134826.7AB is not plotted, given its very unusual properties relative to all other known systems and the large systematic uncertainty in its mass ratio; see Appendix B.)

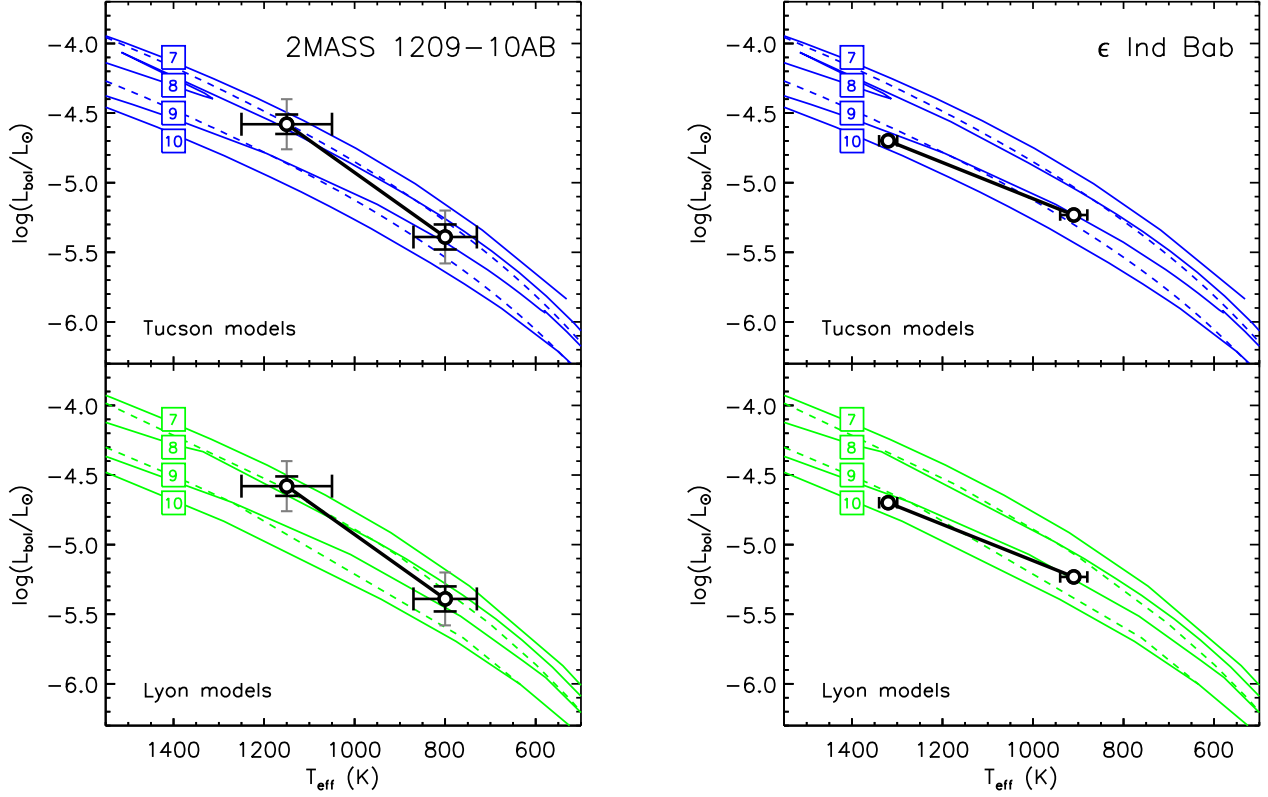


Fig. 6.— H-R diagram showing the two components of 2MASS J1209–1004AB and ϵ Ind Bab compared to isochrones and iso-mass tracks from the Tucson and Lyon (COND) evolutionary models. The data points show the individual components. The thick black diagonal connects the two components, showing the isochrone defined by the binary system. The isochrones are shown as solid colored lines, with the numbers in squares on the left side of the plots giving the logarithms of the isochrone ages ($10^7, 10^8, 10^9, 10^{10}$ yr). The iso-mass tracks for $0.01 M_{\odot}$ (upper line) and $0.04 M_{\odot}$ (lower line) are shown as dashed black lines. For 2MASS J1209–1004AB, two sets of errors are shown for the y -axis: the longer, thinner grey error bars show the total error in the L_{bol} measurements, and the shorter, thicker black errors bars show the errors with the uncertainty in the distance removed, since this uncertainty is common to both components. For ϵ Ind Bab, the plot uses the T_{eff} values from King et al. (2010).

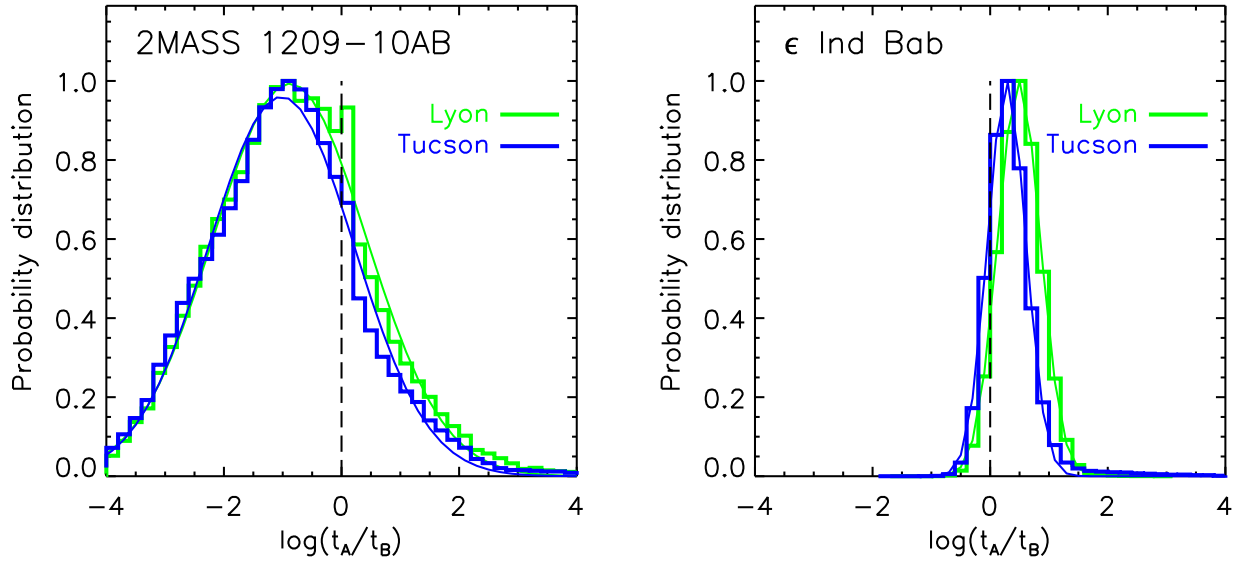


Fig. 7.— Probability distribution of the age difference between components A and B in the 2MASS J1209–1004AB and ϵ Ind Bab systems, based on ages inferred from their locations on the H-R Diagram (Figure 6) and the Lyon (COND) and Tucson evolutionary models. The histogram shows the results from our Monte Carlo calculation, and the thin solid line shows the best fitting Gaussian to the binned probability distribution. The dashed vertical line denotes coevality of the two components.

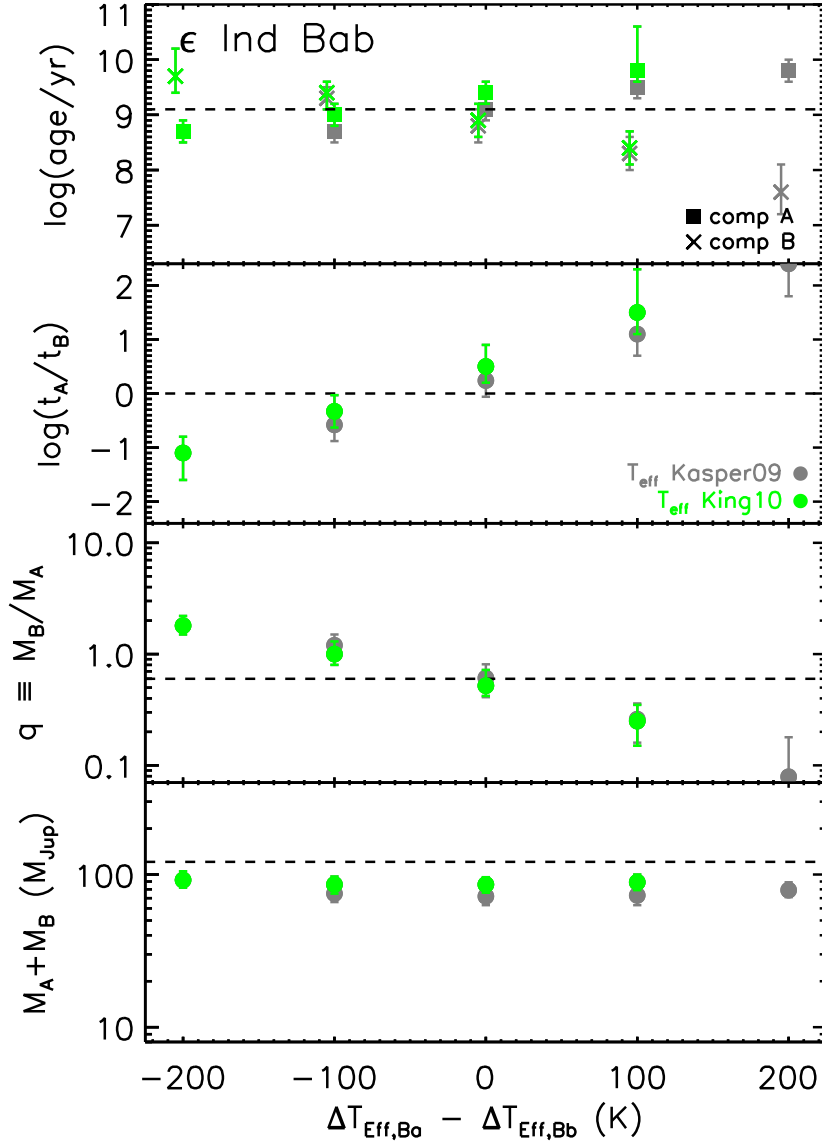


Fig. 8.— The effect of changing the relative T_{eff} values assigned to ϵ Ind Ba and Bb on the physical properties derived from the H-R diagram positions, based on the Lyon/COND evolutionary models. The relative T_{eff} difference between the two components is assumed to be applied with an equal but opposite amplitude to both components. For instance, the leftmost point represents a 50 K decrease in T_{eff} for component Ba and a 50 K increase for component Bb. The four plotted properties are the ages of the individual components, the age difference, the mass ratio, and the total mass. The horizontal dashed lines represent the available constraints: for this system, the age of the primary star ($\log(t/\text{yr}) = 9.1$), the requirement of coevality ($\log(t_A/t_B) = 1$), the mass ratio inferred from the luminosity ratio ($q = 0.6$), and the total dynamical mass ($121 M_{\text{Jup}}$). The grey points are the results based on using the Kasper et al. (2009) T_{eff} 's and the green on the King et al. (2010) T_{eff} 's. The rightmost point is missing for the King et al. (2010) models as such a large temperature change moves the binary components off the loci of available models.

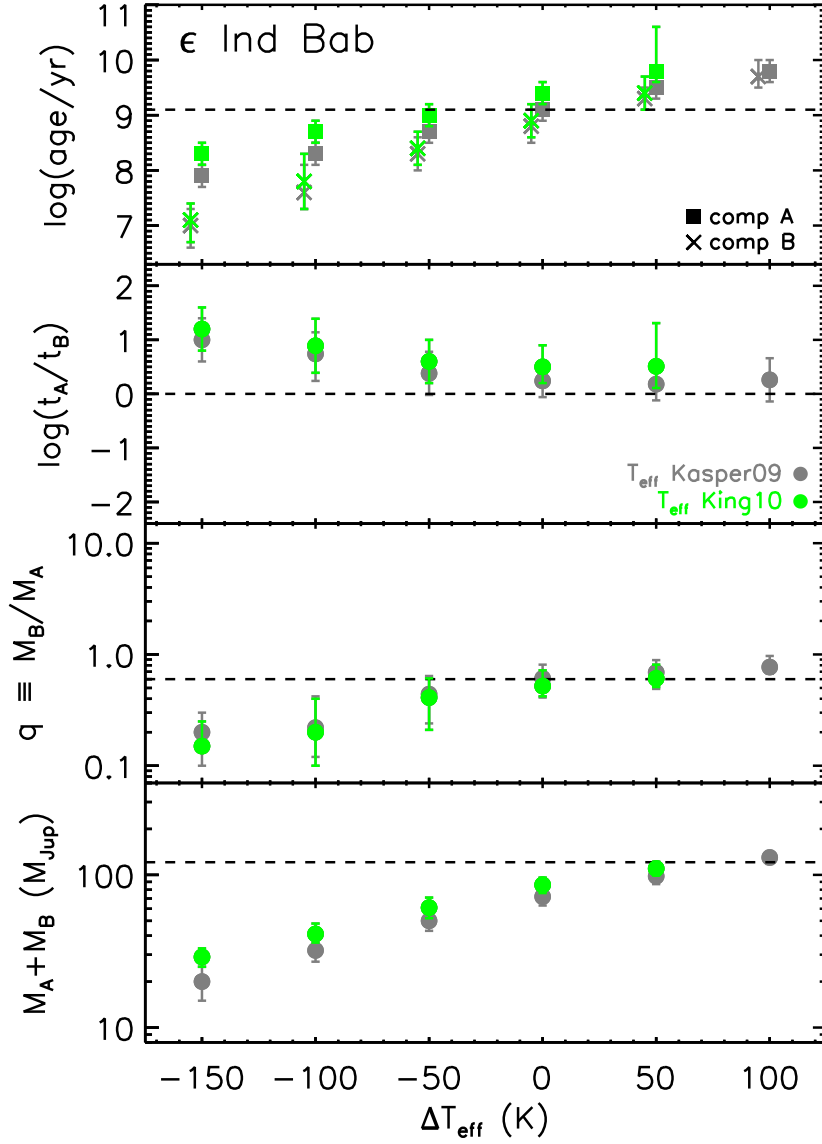


Fig. 9.— The effect of applying a constant offset to the assumed T_{eff} values for ϵ Ind A and ϵ Ind B, with grey being T_{eff} from Kasper et al. (2009) and green from King et al. (2010). For example, the leftmost point represents a 150 K decrease from the nominal T_{eff} values employed in § 4.1. See Figure 8 caption for more details.

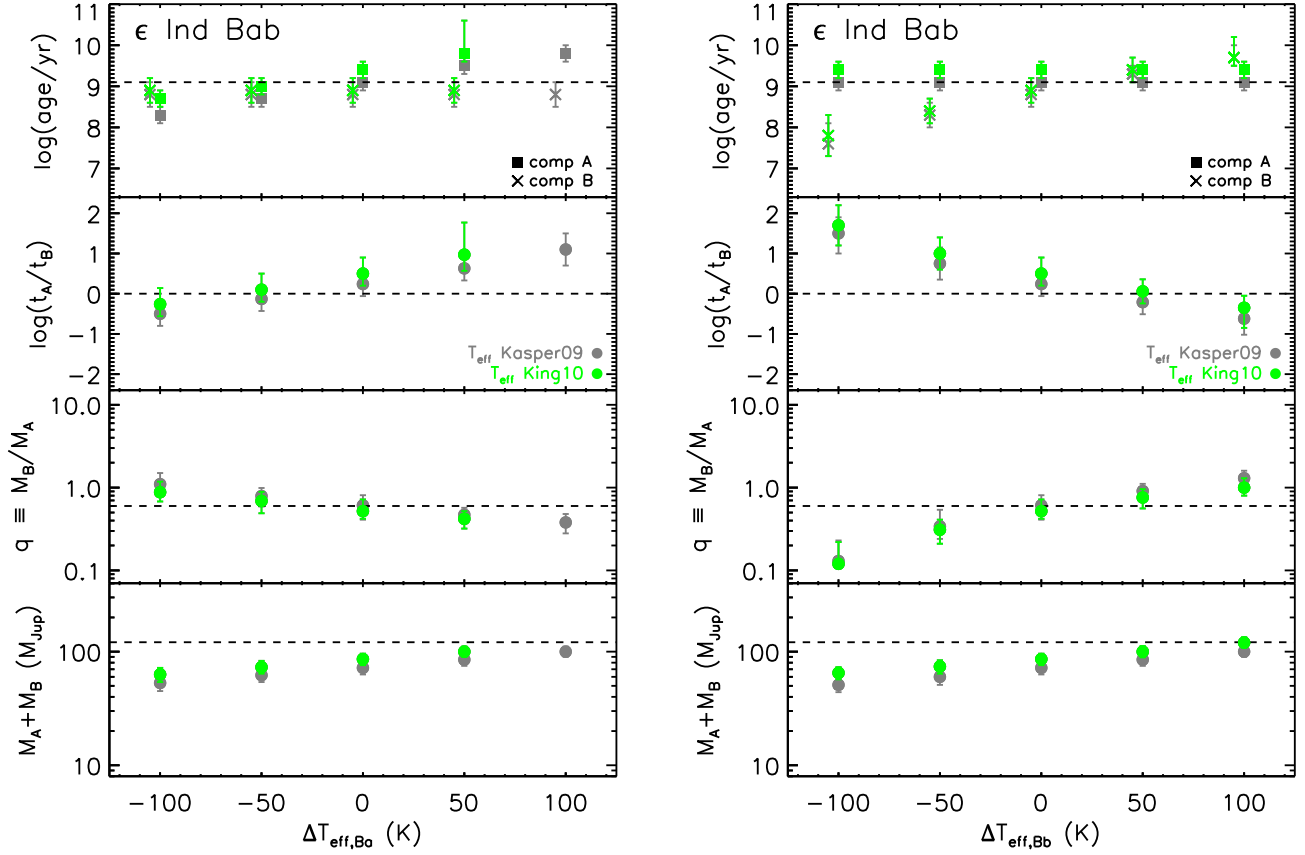


Fig. 10.— The effect of changing the assumed T_{eff} value for one component of ϵ Ind Bab while leaving the T_{eff} of the other component fixed, with grey points from the Kasper et al. (2009) values and green from King et al. (2010). **Left:** Changing the T_{eff} of component Ba. For example, the leftmost point represents a 100 K decrease from the nominal T_{eff} value employed in § 4.1. See Figure 8 caption for more details. **Right:** Changing the T_{eff} of component Bb.

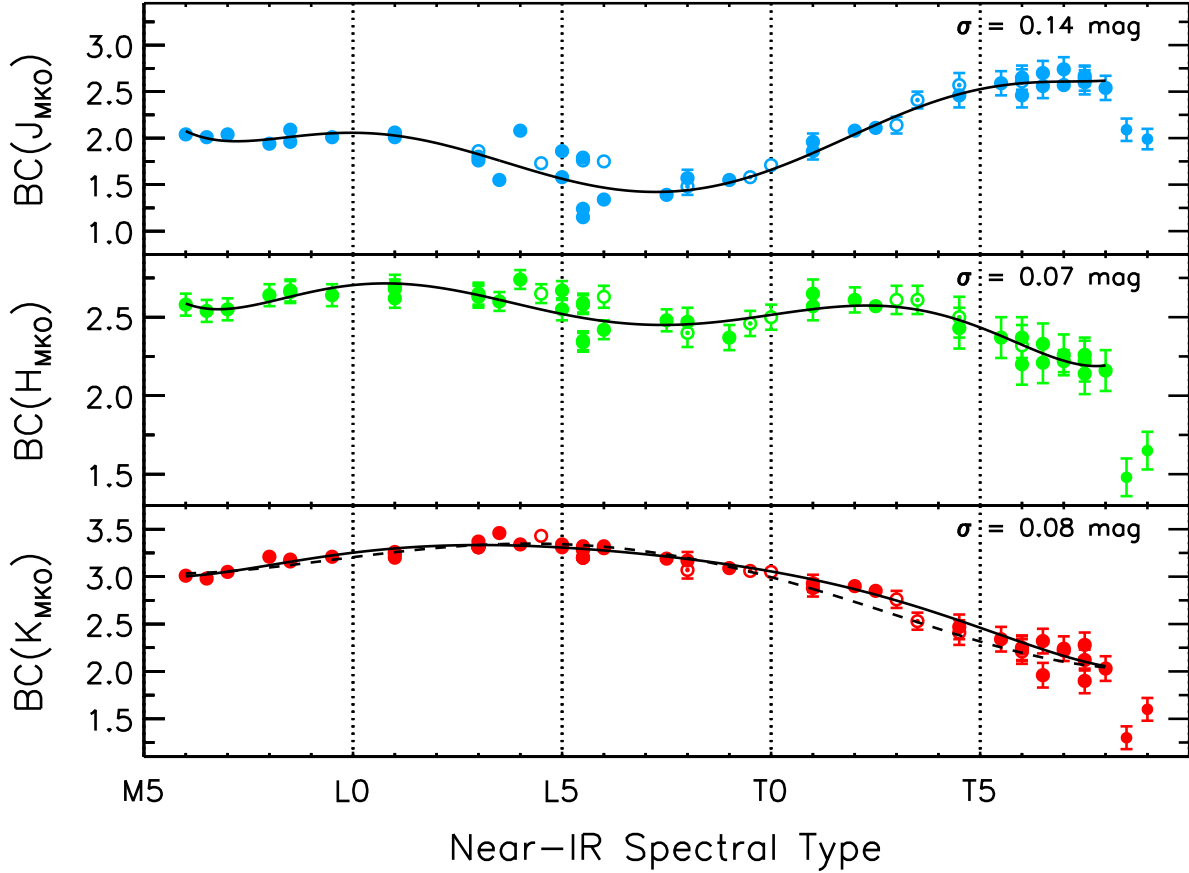


Fig. 11.— Bolometric correction as a function of near-IR spectral type for the MKO J , H , and K -band filters, based on data from Golimowski et al. (2004a), Luhman et al. (2007b), Liu et al. (2007), Leggett et al. (2008), Smart et al. (2010), and Leggett et al. (2010a). Points without visible error bars have uncertainties smaller than the plotting symbol. The solid line overplots a 6th-order polynomial fit to the datasets for objects as cool as T8, with coefficients given in Table 6. The dotted line for the K -band data gives the fit from Golimowski et al. (2004a). Known and suspected binaries are plotted as open circles and as circumscribed small circles, respectively, and excluded from the fits. Suspected binaries are those flagged by Liu et al. (2006) based on their large overluminosity relative to objects of similar spectral type. The L dwarfs are classified on the Geballe et al. (2002) scheme and the T dwarfs on the Burgasser et al. (2006b) scheme. The two coolest objects (T8.5 Wolf 940B and T9 ULAS 0034–0052) are excluded from the fit.

Table 1. Keck LGS AO Observations

Date (UT)	Filter ^a	Airmass	FWHM (mas)	Strehl ratio	Separation (mas)	Position angle (deg)	Δ mag
2007-Apr-22	<i>J</i>	1.46	112 ± 3	0.022 ± 0.002	143 ± 6	311 ± 2	1.5 ± 0.2
	<i>H</i>	1.40	105 ± 5	0.049 ± 0.004	151 ± 13	314 ± 5	2.8 ± 0.3
	<i>K_S</i>	1.53	92 ± 5	0.121 ± 0.019	156 ± 7	314 ± 4	3.2 ± 0.5
2008-Jan-16	<i>CH₄s</i>	1.22	77 ± 5	0.083 ± 0.012	142 ± 7	313 ± 3	2.07 ± 0.17

Note. — All photometry on the MKO system. The tabulated uncertainties on the imaging performance (FWHM and Strehl ratio) are the RMS of the measurements from the individual images.

Table 2. Resolved Properties of 2MASS J1209–1004AB

Property	Component A	Component B
J (mag)	15.80 ± 0.05	17.27 ± 0.17
CH_4s (mag)	15.20 ± 0.04	17.27 ± 0.15
H (mag)	15.32 ± 0.04	18.08 ± 0.26
K_S (mag)	15.12 ± 0.14	18.29 ± 0.53
K (mag)	15.22 ± 0.04	18.48 ± 0.52
$J - H$ (mag)	0.48 ± 0.06	-0.81 ± 0.31
$J - K$ (mag)	0.58 ± 0.07	-1.21 ± 0.54
$CH_4s - H$ (mag)	-0.12 ± 0.05	-0.81 ± 0.30
$H - K$ (mag)	0.10 ± 0.05	-0.40 ± 0.58
Estimated spectral type	$T2.0 \pm 0.5$	$T7.5 \pm 0.5$
d_{phot} (pc)	21 ± 4	
$M(J)$ (mag)	14.19 ± 0.41	15.66 ± 0.44
$M(CH_4s)$ (mag)	13.59 ± 0.41	15.66 ± 0.44
$M(H)$ (mag)	13.71 ± 0.41	16.47 ± 0.49
$M(K_S)$ (mag)	13.51 ± 0.43	16.68 ± 0.67
$M(K)$ (mag)	13.61 ± 0.41	16.87 ± 0.66
$\log(L_{bol,A+B}/L_\odot)$	$-4.61 \pm 0.15(0.02)^a$	
M_{bol} (from J -band)	16.21 ± 0.45	18.24 ± 0.47
$\log(L_{bol}/L_\odot)$ (from J -band)	-4.58 ± 0.18	-5.39 ± 0.19
$\log(L_{bol,A}/L_{bol,B})$ (from J -band)	0.81 ± 0.11	

Note. — All infrared photometry on the MKO photometric system. We also measure integrated-light *Spitzer*/IRAC photometry for the system of $[3.6] = 14.02 \pm 0.03$, $[4.5] = 13.49 \pm 0.03$, $[5.8] = 13.33 \pm 0.03$, and $[8.0] = 13.06 \pm 0.07$ mags (§ 3.6).

^aThe error in parenthesis gives the L_{bol} error assuming there is no uncertainty in the distance.

Table 3. Properties of 2MASS J1209–1004AB Derived from Evolutionary Models

Property	Component A	Component B
$t = 0.5$ Gyr		
Total mass (M_{Jup})	52 ± 7	
Mass (M_{Jup})	36 ± 6	17 ± 4
q ($\equiv M_B/M_A$)	0.47 ± 0.16	
$T_{\text{eff}}(K)$	1281 ± 162	771 ± 103
$T_{\text{eff},B}/T_{\text{eff},A}$	0.60 ± 0.08	
Radius (R_{\odot})	0.101 ± 0.002	0.109 ± 0.003
$\log(g)$ (cgs)	4.96 ± 0.11	4.56 ± 0.13
Orbital period (yr)	27^{+50}_{-10}	
$t = 1$ Gyr		
Total mass (M_{Jup})	75 ± 10	
Mass (M_{Jup})	49 ± 9	25 ± 5
q ($\equiv M_B/M_A$)	0.51 ± 0.10	
$T_{\text{eff}}(K)$	1336 ± 173	802 ± 107
$T_{\text{eff},B}/T_{\text{eff},A}$	0.60 ± 0.07	
Radius (R_{\odot})	0.092 ± 0.002	0.101 ± 0.003
$\log(g)$ (cgs)	5.18 ± 0.11	4.80 ± 0.12
Orbital period (yr)	22^{+42}_{-8}	
$t = 5$ Gyr		
Total mass (M_{Jup})	132 ± 10	
Mass (M_{Jup})	77 ± 5	55 ± 8
q ($\equiv M_B/M_A$)	0.72 ± 0.07	
$T_{\text{eff}}(K)$	1418 ± 163	881 ± 120
$T_{\text{eff},B}/T_{\text{eff},A}$	0.62 ± 0.07	
Radius (R_{\odot})	0.082 ± 0.001	0.083 ± 0.003
$\log(g)$ (cgs)	5.48 ± 0.04	5.31 ± 0.11
Orbital period (yr)	17^{+31}_{-6}	
$t = 10$ Gyr		
Total mass (M_{Jup})	149 ± 8	
Mass (M_{Jup})	79 ± 3	70 ± 7

Table 3—Continued

Property	Component A	Component B
q ($\equiv M_B/M_A$)	0.90 \pm 0.03	
$T_{eff}(K)$	1424 \pm 159	908 \pm 119
$T_{eff,B}/T_{eff,A}$	0.64 \pm 0.07	
Radius (R_\odot)	0.081 \pm 0.002	0.078 \pm 0.002
$\log(g)$ (cgs)	5.50 \pm 0.03	5.47 \pm 0.09
Orbital period (yr)	15.9 ^{+29.4} _{-5.8}	

Table 4. Homogenous Compilation of Substellar Field Binaries

Binary	SpT(A+B)	SpT(A)	SpT(B)	d (pc)	Age (Gyr)	$\log(L_{\text{bol},A})$	$\log(L_{\text{bol},B})$	$\log(\frac{L_{\text{bol},A}}{L_{\text{bol},B}})$	q	References					Notes
										Disc	Phot	SpT	Dist	Age	
DENIS-P J004135.3–562112AB	M8.0 ± 0.5	M6.5 ± 1.0	M9.0 ± 1.0	50 ⁺²¹ ₋₁₀	0.01 (0.005–0.2)	-2.44 ± 0.34(0.03)	-2.78 ± 0.34(0.04)	0.34 ± 0.05	0.74±0.18	55	16, 55	53, 55	55	54	
LP 349-25AB	M8.0 ± 0.5	M7.5 ± 1.0	M8.0 ^{+1.0} _{-1.0}	13.2 ± 0.3	0.127 ^{+0.021} _{-0.017}	-3.04 ± 0.02(0.02)	-3.18 ± 0.03(0.03)	0.13 ± 0.02	0.872 ^{+0.014} _{-0.018}	21	16, 19	19, 23	22	19	a
Gl 569Bab	M8.5 ± 0.5	M8.5 ± 0.5	M9.0 ± 0.5	9.65 ± 0.16	0.46 ^{+0.11} _{-0.07}	-3.42 ± 0.02(0.02)	-3.62 ± 0.02(0.02)	0.20 ± 0.02	0.866 ^{+0.019} _{-0.014}	46	19, 36	28, 36	61	19	a
DENIS-P J035726.9–441730AB	L0.0 ± 0.5	M9.0 ± 0.5	L1.5 ± 0.5	40 ± 7	~0.1	-3.58 ± 0.15(0.04)	-3.77 ± 0.15(0.04)	0.19 ± 0.05	0.87±0.03	3	4, 16	15, 47		15	b
Kelu-1AB	L2.0 ± 0.5	L2.0 ± 0.5	L3.5 ± 0.5	18.7 ± 0.7	0.5 (0.3–0.8)	-3.82 ± 0.05(0.04)	-4.00 ± 0.05(0.04)	0.18 ± 0.04	0.92±0.02	39	37, 39	31	17	39	
2MASS J11463449+2230527AB	L3.0 ± 0.5	L3.0 ± 0.5	L3.0 ± 1.0	27.2 ± 0.6	0.5 (0.3–0.8)	-3.82 ± 0.04(0.04)	-3.96 ± 0.04(0.04)	0.13 ± 0.05	0.94±0.02	50	4, 16	31	17	1	b,c
SDSS J224953.47+004404.6AB	L3.0 ± 1.0	L3.0 ± 0.5	L5.0 ± 1.0	53 ± 15	0.1 (0.02–0.3)	-3.9 ± 0.3(0.03)	-4.2 ± 0.3(0.04)	0.36 ± 0.02	0.75±0.10	2	2, 34	2, 27	2	2	
2MASS J00250365+4759191AB	L4.0 ± 1.0	L4.0 ± 1.0	L4.5 ^{+2.0} _{-1.0}	25 ± 7	0.3 (0.1–0.5)	-4.08 ± 0.20(0.04)	-4.13 ± 0.22(0.04)	0.06 ± 0.06	0.96±0.04	51	9, 16, 51	14		20	d
HD 130948BC	L4.0 ± 1.0	L4.0 ± 1.0	L4.0 ± 1.0	18.17 ± 0.11	0.79 ^{+0.22} _{-0.23}	-3.82 ± 0.05(0.04)	-3.90 ± 0.05(0.04)	0.08 ± 0.01	0.948±0.005	49	18	26	61	18	a
Gl 417BC	L4.5 ± 0.5	L4.5 ± 0.5	L4.5 ^{+1.0} _{-0.5}	21.9 ± 0.2	0.74 (0.58–0.86)	-4.06 ± 0.03(0.03)	-4.18 ± 0.04(0.04)	0.12 ± 0.05	0.94±0.02	3	16, 42	32	61	2	
GJ 1001BC	L5.0 ± 0.5	L5.0 ± 0.5	L5.0 ± 1.0	13.0 ^{+0.7} _{-0.6}	3 (1–10)	-4.03 ± 0.06(0.05)	-4.08 ± 0.07(0.05)	0.05 ± 0.08	0.99±0.01	25	16, 25	33	29	38	e
DENIS-P J1228.2–1547AB	L5.0 ± 0.5	L5.0 ± 0.5	L5.0 ± 1.0	20.2 ^{+0.8} _{-0.7}	19 ± 4	-4.19 ± 0.05(0.03)	-4.24 ± 0.05(0.04)	0.05 ± 0.05	0.98±0.03	35, 45	16, 42	31	17		
2MASS J12392727+5515371AB	L5.0 ± 0.5	L5.0 ± 0.5	L6.0 ^{+2.5} _{-1.5}	19 ± 4		-4.23 ± 0.17(0.04)	-4.31 ± 0.17(0.06)	0.09 ± 0.07	0.95±0.05	24	3, 16	32			b
2MASS J21321145+1341584AB	L6.0 ± 0.5	L5.0 ± 0.5	L7.5 ± 0.5	23 ± 4		-4.39 ± 0.17(0.04)	-4.72 ± 0.17(0.04)	0.33 ± 0.04	0.76±0.03	58	16, 58	14, 58			
2MASS J17281150+3948593AB	L7.0 ± 0.5	L7.0 ± 0.5	L9.0 ^{+2.0} _{-1.0}	24 ± 2		-4.47 ± 0.08(0.04)	-4.65 ± 0.08(0.04)	0.18 ± 0.04	0.85±0.03	24	16, 42	32	62		
2MASS J08503593+1057156AB	L6.0 ± 0.5	L6.0 ± 0.5	L9.5 ± 1.0	26 ⁺³ ₋₂		-4.53 ± 0.08(0.03)	-4.87 ± 0.09(0.03)	0.34 ± 0.04	0.75±0.03	50	37, 42	31	17		
2MASS J22551861–5713056AB	L6.0 ± 1.0	L5.0 ± 1.0	L8.0 ± 1.0	12 ± 3		-4.38 ± 0.20(0.04)	-4.95 ± 0.22(0.07)	0.57 ± 0.09	0.63±0.05	53	9, 16, 51	53			
2MASS J21522609+0937575AB	L6.0 ± 1.0	L6.0 ± 1.0	L8.5 ^{+4.0} _{-3.0}	22 ± 5		-4.36 ± 0.19(0.04)	-4.39 ± 0.20(0.04)	0.03 ± 0.05	0.98±0.04	51	16, 51	53			
SDSS J141624.08+134826.7AB	L6.0 ± 0.5	L6.0 ± 0.5	T7.5 ± 0.5	8 ⁺² ₋₁		-4.30 ± 0.20(0.03)	-6.24 ± 0.20(0.03)	1.94 ± 0.04	0.18±0.01	12	12	5, 12	57		f
DENIS-P J225210.7–173013AB	L7.5 ± 1.0	L4.5 ± 1.0	T4.5 ± 1.0	11 ± 2		-4.51 ± 0.18(0.04)	-4.93 ± 0.18(0.04)	0.42 ± 0.05	0.70±0.03	52	9, 16, 42, 51	11, 30			g
2MASS J05185995–2828372AB	T1.0 ± 0.5	L7.5 ± 0.5	T5.0 ± 0.5	20 ± 4		-4.55 ± 0.19(0.10)	-5.29 ± 0.23(0.15)	0.75 ± 0.22	0.54±0.10	9	9, 16	10, 11			
SDSS J042348.57–041403.5AB	T0.0 ± 0.5	L7.5 ± 0.5	T2.0 ± 0.5	15.2 ± 0.4		-4.33 ± 0.04(0.03)	-4.59 ± 0.04(0.03)	0.26 ± 0.04	0.80±0.03	7	9, 37	10, 11	62		
DENIS-P J020529.0–115925AB	L7.0 ± 0.5	L7.0 ± 0.5	L6.0 ± 1.0	19.8 ± 0.6		-4.28 ± 0.04(0.04)	-4.34 ± 0.05(0.04)	0.06 ± 0.05	0.96±0.03	35	16, 42	31	17		
2MASS J09153413+0422045AB	L6.0 ± 1.0	L6.0 ± 1.0	L7.0 ^{+3.0} _{-1.5}	18 ± 5		-4.28 ± 0.20(0.04)	-4.33 ± 0.20(0.04)	0.05 ± 0.05	0.97±0.04	51	9, 16, 42, 51	53			
2MASS J21011544+1756586AB	L7.5 ± 0.5	L7.5 ± 0.5	T1.0 ^{+2.0} _{-2.5}	33 ⁺⁴ ₋₃		-4.55 ± 0.11(0.04)	-4.67 ± 0.13(0.08)	0.13 ± 0.09	0.89±0.07	3	3, 13	32	62		b
2MASS J03105986+1648155AB	L8.0 ± 0.5	L8.0 ± 0.5	L9.0 ^{+2.5} _{-1.5}	25 ± 4		-4.54 ± 0.15(0.03)	-4.60 ± 0.15(0.04)	0.06 ± 0.04	0.95±0.03	59	37, 42	32			
Gl 337CD	T0.0 ± 0.5	T0.0 ± 0.5	T0.5 ^{+1.5} _{-2.0}	20.4 ± 0.2	1.5 (0.6–3.4)	-4.62 ± 0.04(0.04)	-4.70 ± 0.05(0.05)	0.08 ± 0.04	0.93±0.03	8	16, 42	10, 63	61	63	
2MASS J09201223+3517429AB	T0.0 ± 0.5	T0.0 ± 0.5	T1.0 ^{+2.5} _{-2.0}	18 ± 3		-4.75 ± 0.15(0.04)	-4.84 ± 0.15(0.04)	0.09 ± 0.05	0.93±0.04	50	16, 42	10, 32			h
SDSS J105213.51+442255.7AB	T0.5 ± 1.0	T0.5 ± 1.0	T0.5 ^{+2.5} _{-2.0}	22 ± 4		-4.76 ± 0.16(0.03)	-4.78 ± 0.16(0.04)	0.02 ± 0.05	0.98±0.04	42	13, 42	13			
SDSS J205235.31–160929.8AB	T1.0 ± 1.0	T1.0 ± 1.0	T3.5 ^{+1.5} _{-2.0}	25 ± 5		-4.74 ± 0.16(0.03)	-4.85 ± 0.16(0.04)	0.12 ± 0.05	0.90±0.04	42	13, 42	13			
2MASS J14044948–3159330AB	T2.5 ± 0.5	T0.0 ± 0.5	T5.0 ± 0.5	18 ± 3		-4.84 ± 0.16(0.05)	-4.99 ± 0.16(0.05)	0.16 ± 0.06	0.88±0.04	44	44	11, 43			
SDSS J102109.69–030420.1AB	T3.0 ± 0.5	T1.0 ± 0.5	T5.0 ± 0.5	29 ⁺⁵ ₋₃		-4.58 ± 0.13(0.04)	-4.75 ± 0.13(0.05)	0.17 ± 0.06	0.86±0.05	9	9, 37, 42	10, 11	60		
ε Ind Bab	T2.5 ± 0.5	T1.0 ± 0.5	T6.0 ± 0.5	3.622 ± 0.004	2 (0.5–7.0)	-4.62 ± 0.03(0.03)	-5.24 ± 0.04(0.04)	0.61 ± 0.05	0.63±0.02	48	16, 48	10, 48, 56	61	1	
SDSS J153417.05+161546.1AB	T3.5 ± 0.5	T1.5 ± 0.5	T5.0 ± 0.5	31 ± 6		-4.87 ± 0.16(0.03)	-5.09 ± 0.16(0.04)	0.23 ± 0.05	0.83±0.03	40	13, 40	40			
2MASS J12095613–1004008AB	T3.0 ± 0.5	T2.0 ± 0.5	T7.5 ± 0.5	21 ± 4		-4.58 ± 0.18(0.07)	-5.39 ± 0.19(0.09)	0.81 ± 0.11	0.51±0.05	1	1, 13	1, 10			
SDSS J092615.38+584720.9AB	T4.5 ± 0.5	T4.5 ± 0.5	T3.0 ^{+2.5} _{-4.0}	22 ± 4		-4.79 ± 0.16(0.06)	-4.95 ± 0.21(0.08)	0.16 ± 0.13	0.88±0.09	9	9, 37	10			
2MASS J15344984–2952274AB	T5.0 ± 0.5	T5.0 ± 0.5	T5.5 ± 0.5	13.6 ± 0.2	0.78 ^{+0.09} _{-0.09}	-5.02 ± 0.02(0.02)	-5.09 ± 0.02(0.02)	0.08 ± 0.02	0.936±0.012	6	34, 41	10, 41	60	41	a
2MASS J12255432–2739476AB	T6.0 ± 0.5	T6.0 ± 0.5	T7.5 ± 0.5	13.3 ^{+0.5} _{-0.4}		-4.93 ± 0.05(0.05)	-5.47 ± 0.05(0.04)	0.54 ± 0.06	0.63±0.03	6	37, 42	10	60		
2MASS J15530228+1532369AB	T7.0 ± 0.5	T7.0 ± 0.5	T7.5 ± 0.5	11 ± 3		-5.42 ± 0.24(0.04)	-5.54 ± 0.25(0.03)	0.12 ± 0.05	0.90±0.05	9	9, 34, 42	10			

Note. — Field binaries are included in this table if the primary spectral type is L4 or later, or if there is other evidence that the system is young enough to be substellar, i.e., from accretion signatures (DENIS-P J0041–56AB), lithium absorption (Kelu-1 and 2MASS J1146+22AB), low surface gravity (DENIS-P J0357–44AB and SDSS J2249+00AB), or dynamical masses (LP 349-25AB and Gl 569Bab). Distance references are listed for objects with trigonometric parallaxes or those with a wide main-sequence companion with a good distance estimate; otherwise the distances are photometric estimates derived by us, except DENIS-P J0041–56AB comes from Reiners (2009). The uncertainties on L_{bol} are listed with and without the uncertainty in the distance folded in. Other notes: (a) The mass ratios come from the published analysis using the measured total dynamical mass and bolometric luminosity of the system combined with the luminosity ratio of the two components. (b) The K -band flux ratio was estimated from $F814W$ -band flux ratio (Appendix B). (c) The age estimate assigned by us is based on the presence of lithium and the L_{bol} of the components using evolutionary models (e.g., Liu & Leggett 2005). (d) This object also has a distance estimate from a comoving wide F8 companion star (G 171-58) of 42.2^{+2.0}_{-1.8} pc (Faherty et al. 2010), which is somewhat discrepant with our photometric distance listed here. (e) GJ 1001BC has an integrated light spectral type of L5.0±0.5 and essentially identical fluxes and colors; thus both components are likely to be L5 (Golimowski et al. 2004b). The absolute magnitudes of component C formally given

to a spectral type of $L4.0\pm 1.0$ using our methodology in Appendix B, which is consistent. We adopt $L5.0\pm 0.5$ for both components. (f) Burningham et al. (2010) and Burgasser et al. (2010b) find the secondary is high gravity and low temperature and suggest an age of ~ 10 Gyr and 2–10 Gyr, respectively. For an age of 10 Gyr, the mass ratio of the binary would be ≈ 0.5 , based on their mass estimates for component B and that of Bowler et al. (2010) for component A. (g) We list the IR spectral type, as an optical type is not available for this object. (h) This has very disparate integrated-light spectral types, L6.5 in the optical and T0 in the near-IR. We use the IR type here.

References. — (1) This work; (2) Allers et al. 2010; (3) Bouy et al. 2003; (4) Bouy et al. 2008; (5) Bowler et al. 2010; (6) Burgasser et al. 2003; (7) Burgasser et al. 2005c; (8) Burgasser et al. 2005a; (9) Burgasser et al. 2006d; (10) Burgasser et al. 2006c; (11) Burgasser et al. 2010a; (12) Burningham et al. 2010; (13) Chiu et al. 2006; (14) Cruz et al. 2007; (15) Cruz et al. 2009; (16) Cutri et al. 2003; (17) Dahn et al. 2002; (18) Dupuy et al. 2009b; (19) Dupuy et al. 2010; (20) Faherty et al. 2010; (21) Forveille et al. 2005; (22) Gatewood & Coban 2009; (23) Gizis et al. 2000; (24) Gizis et al. 2003; (25) Golimowski et al. 2004b; (26) Goto et al. 2002; (27) Hawley et al. 2002; (28) Henry & Kirkpatrick 1990; (29) Henry et al. 2006; (30) Kendall et al. 2004; (31) Kirkpatrick et al. 1999; (32) Kirkpatrick et al. 2000; (33) Kirkpatrick et al. 2001; (34) Knapp et al. 2004; (35) Koerner et al. 1999; (36) Lane et al. 2001; (37) Leggett et al. 2002b; (38) Leggett et al. 2002a; (39) Liu & Leggett 2005; (40) Liu et al. 2006; (41) Liu et al. 2008; (42) Liu et al., in prep; (43)Looper et al. 2007; (44) Looper et al. 2008; (45) Martín et al. 1999; (46) Martín et al. 2000; (47) Martín et al. 2006; (48) McCaughrean et al. 2004; (49) Potter et al. 2002; (50) Reid et al. 2001; (51) Reid et al. 2006a; (52) Reid et al. 2006b; (53) Reid et al. 2008; (54) Reiners 2009; (55) Reiners et al. 2010; (56) Scholz et al. 2003; (57) Scholz 2010; (58) Siegler et al. 2007; (59) Stumpf et al. 2010; (60) Tinney et al. 2003; (61) van Leeuwen 2007; (62) Vrba et al. 2004; (63) Wilson et al. 2001.

Table 5. Ages and Masses Inferred from the H-R Diagram

$T_{eff,A}^{atm}, T_{eff,B}^{atm}$	Model	$\log(t_A/\text{yr})$	$\log(t_B/\text{yr})$	$\log(t_A/t_B)$	M_A (M_{Jup})	M_B (M_{Jup})	$M_B + M_A$ (M_{Jup})	$q \equiv M_B/M_A$
2MASS J1209–1004AB								
$1150 \pm 100 \text{ K}, 800 \pm 70 \text{ K}$ (this work)	Lyon/COND	$7.5_{-1.5}^{+1.2}$	$8.5_{-1.5}^{+1.0}$	$-0.8_{-1.3}^{+1.3}$	10_{-7}^{+16}	18_{-13}^{+25}	34_{-19}^{+27}	$1.7_{-1.3}^{+5.2}$
	Tucson	$7.6_{-1.5}^{+1.2}$	$8.8_{-1.7}^{+1.1}$	$-1.0_{-1.3}^{+1.2}$	11_{-8}^{+24}	20_{-17}^{+43}	36_{-25}^{+63}	$1.6_{-1.3}^{+6.2}$
ϵ Ind Bab								
$1275 \pm 25 \text{ K}, 900 \pm 25 \text{ K}$ (Kasper et al. 2009)	Lyon/COND	9.1 ± 0.2	8.8 ± 0.3	0.2 ± 0.3	44_{-6}^{+8}	27_{-7}^{+7}	72_{-9}^{+10}	0.6 ± 0.2
	Tucson	9.1 ± 0.2	9.0 ± 0.2	0.1 ± 0.3	49 ± 8	28_{-7}^{+8}	78_{-10}^{+11}	0.6 ± 0.2
$1320 \pm 20 \text{ K}, 910 \pm 30 \text{ K}$ (King et al. 2010)	Lyon/COND	9.4 ± 0.2	8.9 ± 0.3	$0.5_{-0.3}^{+0.4}$	57 ± 7	30 ± 8	86_{-10}^{+11}	$0.52_{-0.14}^{+0.17}$
	Tucson	9.3 ± 0.2	9.0 ± 0.3	$0.3_{-0.4}^{+0.3}$	63_{-7}^{+8}	31_{-9}^{+11}	95_{-12}^{+13}	$0.49_{-0.14}^{+0.19}$

Note. — The results for each component are the median and 68% confidence limits from the Monte Carlo-generated probability distributions for the ages and masses computed from the H-R diagram positions (§ 4).

Table 6. Coefficients of Polynomial Fits for Bolometric Correction Versus Near-IR Spectral Type

Bandpass	c_0	c_1	c_2	c_3	c_4	c_5	c_6	RMS (mag)
J_{MKO}	1.890448e+01	-8.053993e+00	1.491738e+00	-1.367605e-01	6.540717e-03	-1.558986e-04	1.462266e-06	0.14
H_{MKO}	1.366709e+01	-5.426683e+00	1.027185e+00	-9.618535e-02	4.733874e-03	-1.171595e-04	1.148133e-06	0.07
K_{MKO}	5.795845e+00	-1.471358e+00	2.868014e-01	-2.647474e-02	1.282657e-03	-3.177629e-05	3.159780e-07	0.08

Note. — These are the coefficients of the 6th-order polynomial fits plotted in Figure 11 for the bolometric correction as a function of near-IR spectral type. The fit for filter X is defined as

$$BC(X) = \sum_{i=0}^6 c_i \times (SpT)^i$$

where the numerical spectral type is defined as $SpT = 11$ for L1, $SpT = 12$ for L2, $SpT = 20$ for T0, etc. The fits are applicable from M6 to T8.5. The L dwarfs are classified on the Geballe et al. (2002) scheme and the T dwarfs on the Burgasser et al. (2006b) scheme. The last column gives the standard deviation about the fit in magnitudes.